




RESEARCH ARTICLE

Disturbance observer-based fixed-time control for hypersonic morphing vehicles with uncertainties

H. Zhang¹, P. Wang¹, G. Tang¹ and W. Bao²

¹National University of Defense Technology, College of Aerospace Science and Engineering, China and ²China Aerospace Science & Technology Corporation, Beijing, China

Corresponding author: P. Wang; Email: wonderful2035@163.com

Received: 24 August 2023; **Revised:** 18 November 2023; **Accepted:** 7 December 2023

Keywords: hypersonic morphing vehicle; fixed-time control; multivariable sliding mode manifold; fuzzy control; fuzzy fixed-time disturbance observer

Abstract

The attitude-tracking problem of hypersonic morphing vehicles (HMVs) is investigated in this research. After introducing variable-span wings, the optimal aerodynamic shape is available throughout the entire flight mission. However, the morphing wings cause significant changes in aerodynamic coefficients and mass distribution, challenging the attitude control. Therefore, a complete design procedure for the flight control system is proposed to address the issue. Firstly, the original model and the control-oriented model of HMVs are built. Secondly, in order to eliminate the influence caused by the multisource uncertainties, an adaptive fixed-time disturbance observer combined with fuzzy control theory is established. Thirdly, the fixed-time control method is developed to stabilise hypersonic morphing vehicles based on a multivariable sliding mode manifold. The control input can be obtained directly. Finally, the effectiveness of the proposed method is proved with the help of the Lyapunov theory and simulation results.

Nomenclature

HMV	Hypersonic morphing vehicle
HFV	Hypersonic flight vehicle
ADRC	Active disturbance rejection control
FDO	Fixed-time disturbance observer
AFFDO	Adaptive fuzzy fixed-time disturbance observer
FTC	Fixed-time control

1.0 Introduction

One of the strengths of hypersonic morphing vehicles (HMVs) is their adaptation to various flight missions and environments [1]. Compared with conventional hypersonic flight vehicles (HFVs), HMVs constantly change their aerodynamic shape to obtain optimal aerodynamic characteristics [2, 3]. Further, the acquired aerodynamic forces and moments are conducive to enhancing flight efficiency and manoeuvrability [3].

However, it is frustrating that the design procedure of the control system is more difficult after introducing the span morphing technology into HFVs [4]. The significant changes in aerodynamic characteristics demand strong robustness and adaptation of the control system [5]. Moreover, the properties, such as the mass distribution, the inertia of moment, and additional moments, vary rapidly, significantly impacting the attitude control. When HMVs perform a flight mission with continuous span morphing, the multisource uncertainties that consist of external disturbances, un-modelled aerodynamics, and

aerodynamic perturbation may cause crucial control issues [6, 7]. Therefore, it is necessary to consider the impact of the multisource uncertainties since the control failure may occur in the morphing phase.

The anti-disturbance methods are long-term developed for robustness enhancement [8, 9]. Worldwide researchers propose many disturbance compensation methods, such as active disturbance rejection control (ADRC) and adaptive compensator [10, 11]. Some other researchers take full advantage of robust controllers to passively suppress disturbances. The observers-based method is regarded as an active way to compensate for the disturbance, which is popular in the controller design for HMVs [12, 13]. The commonly used methods are nonlinear disturbance observer and extended state observer [14]. Both disturbance estimation strategies are introduced in the flight control system for disturbance compensation [15]. Though the conventional nonlinear disturbance observer has achieved fruitful applications, there still exists opportunities to enhance the performance [16]. The first point is combining the disturbance observer with the fixed/finite-time control method to achieve a fast and high-accuracy anti-disturbance attitude control system [17]. The other is introducing intelligent control methods, such as a fuzzy logic system, neural network, and iterative learning method, to increase the intelligent level of flight control [18, 19]. Such research motivates us to develop a novel fixed-time disturbance observer (FDO), named adaptive fuzzy fixed-time disturbance observer (AFFDO) [20–23].

The most important work is to design a robust controller for attitude angle tracking, which is especially demanded in morphing phases. It is necessary to make deliberate choices, even though a large selection of control methods is available for HFVs [24, 25]. The sliding mode control is always adopted to develop robust controllers for hypersonic vehicles because of its robustness. In past decades, the asymptotically stable system theory has always been chosen in sliding mode flight controllers. To enhance the convergence performance, finite/fixed-time stability is developed [26]. The fixed-time control (FTC) method stands out because of its outstanding convergence rate and the scalable controller structure [27]. Moreover, unlike the finite-time control method, the fixed-time controller forces the closed-loop system to converge in the fixed time, which is related to some controller parameters instead of the initial value of the HMV system [28, 29]. Therefore, combining the sliding mode control and fixed-time control is a wise way to derive a robust controller [30].

Based on the above discussions, this paper focuses on proposing a fixed-time control technique integrated with the anti-uncertainty technique for the hypersonic morphing vehicle. Strong robustness is demanded to deal with the multisource uncertainties and the rapid aerodynamic characteristics variation in the morphing phase. Therefore, a fixed-time controller combined with an adaptive fuzzy fixed-time disturbance observer is presented for HMVs. Hypersonic flights in morphing phases is adopted to build the test scenario since the aerodynamic changes are significant. The major contributions in this paper are as follows.

- 1) A fixed-time flight control strategy is developed for HMVs. The designed procedure fully utilises the multivariable sliding mode manifold and homogenous system theory. Unlike the traditional fixed-time methods [37], the proposed controllers will lead to a more explicit settling time instead of a complex expression with many parameters. Thus, one can pre-assign the settling time in the controller design.
- 2) An adaptive fuzzy fixed-time disturbance observer is developed. The multisource uncertainty can be exactly estimated. Unlike the super-twisting algorithm-based fixed-time disturbance observer [37], the designed disturbance observer does not require the knowledge of disturbance derivatives. Thus, the application of the AFFDO in actual hypersonic flights with unknown disturbances could be promoted.
- 3) The proposed control design scheme gets rid of the decoupling issue, and the control input is directly obtained instead of traditional inner-loop and outer-loop designs.
- 4) Since the aerodynamic changes are significant, hypersonic flights in the continuous morphing stage are employed to build the simulation case. By using the simulations, the performance will be analysed.

2.0 Preparations and system transformation

2.1 Model of hypersonic morphing vehicle

This section introduces the hypersonic vehicle model with morphing-span wings. The effect of variable span wings is included in the aerodynamics. Meanwhile, all the configurations can be found in [1].

2.1.1 Model of hypersonic morphing vehicle

The model of the hypersonic morphing vehicle is given below.

$$\left\{ \begin{aligned} \dot{\alpha} &= -\omega_x \cos \alpha \tan \beta + \omega_y \sin \alpha \tan \beta \\ &\quad + \omega_z - \frac{L}{mV \cos \beta} + \frac{g}{V \cos \beta} \cos \theta \cos \gamma_V \\ \dot{\beta} &= \omega_x \sin \alpha + \omega_y \cos \alpha + \frac{N}{mV} + \frac{g}{V} \cos \theta \sin \gamma_V \\ \dot{\gamma}_V &= \omega_x \cos \alpha \sec \beta - \omega_y \sin \alpha \sec \beta \\ &\quad + \frac{(\tan \beta + \tan \theta \sin \gamma_V) L + N \tan \theta \cos \gamma_V}{mV} \\ &\quad + \frac{g}{V} \cos \theta \tan \beta \sin \gamma_V \end{aligned} \right. \tag{1}$$

$$\left\{ \begin{aligned} \dot{\omega}_x &= I_x^{-1}(M_x + M_{sx}) + I_x^{-1}(I_y - I_z) \omega_y \omega_z - I_x^{-1} \dot{I}_x \omega_x \\ \dot{\omega}_y &= I_y^{-1}(M_y + M_{sy}) + I_z^{-1}(I_z - I_x) \omega_z \omega_x - I_y^{-1} \dot{I}_y \omega_y \\ \dot{\omega}_z &= I_z^{-1}(M_z + M_{sz}) + I_z^{-1}(I_x - I_y) \omega_x \omega_y - I_z^{-1} \dot{I}_z \omega_z \end{aligned} \right. \tag{2}$$

where α , β and γ_V represent the attack angle, sideslip angle and bank angle, respectively. ω_x , ω_y and ω_z indicate the rolling angle rate, yawing angle rate and pitching angle rate, respectively. L , D and N represent the lift force, the drag force and the lateral force. V , m and g denote the flight velocity, the mass and the gravitational acceleration. M_x , M_y and M_z stand for the roll, yaw, pitch moment. M_{sx} , M_{sy} and M_{sz} are the additional moments directly caused by the span variant. I_x , I_y and I_z are roll, pitch and yaw moment of inertia. The forces and moments can be described as follows.

$$\left\{ \begin{aligned} L &= qS_0 \bar{C}_L \\ D &= qS_0 \bar{C}_D \\ N &= qS_0 \bar{C}_N \end{aligned} \right. \tag{3}$$

$$\left\{ \begin{aligned} M_x &= qS_0 L_1 \bar{m}_x \\ M_y &= qS_0 L_1 \bar{m}_y \\ M_z &= qS_0 L_2 \bar{m}_z \end{aligned} \right. \tag{4}$$

where \bar{m}_x , \bar{m}_y and \bar{m}_z represent the equivalent roll, yaw and pitch moment coefficient, respectively. \bar{C}_L , \bar{C}_N and \bar{C}_D denote the equivalent aerodynamic force coefficients. q is dynamic pressure.

The aerodynamic parameters are listed as

$$\left\{ \begin{aligned} \bar{C}_i(\xi) &= \frac{S(\xi) C_i(\xi)}{S_0}, i = L, D, N \\ \bar{m}_i(\xi) &= \frac{S(\xi) m_i(\xi)}{S_0}, i = x, y, z \end{aligned} \right. \tag{5}$$

$$\begin{cases} \bar{C}_L = C_{L, Ma, \alpha}^{\delta_x} \cdot \delta_{x,L} + C_{L, Ma, \alpha}^{\delta_y} \cdot \delta_{y,L} + C_{L, Ma, \alpha}^{\delta_z} \cdot \delta_{z,L} + C_{L, Ma, \alpha}^{\xi} \cdot \xi_L \\ \bar{C}_D = C_{D, Ma, \alpha}^{\delta_x} \cdot \delta_{x,D} + C_{D, Ma, \alpha}^{\delta_y} \cdot \delta_{y,D} + C_{D, Ma, \alpha}^{\delta_z} \cdot \delta_{z,D} + C_{D, Ma, \alpha}^{\xi} \cdot \xi_D \\ \bar{C}_N = C_{N, Ma, \alpha}^{\beta} \cdot \beta_N + C_{N, Ma, \alpha}^{\delta_y} \cdot \delta_{y,N} \\ \bar{m}_x = m_{x, Ma, \alpha}^{\beta} \cdot \beta_{mx} + m_{x, Ma, \alpha}^{\delta_x} \cdot \delta_{x,mx} \\ \bar{m}_y = m_{y, Ma, \alpha}^{\beta} \cdot \beta_{my} + m_{y, Ma, \alpha}^{\delta_y} \cdot \delta_{y,my} \\ \bar{m}_z = m_{z, Ma, \alpha}^{\delta_x} \cdot \delta_{x,mz} + m_{z, Ma, \alpha}^{\delta_z} \cdot \delta_{z,mz} + m_{z, Ma, \alpha}^{\xi} \cdot \xi_{mz} \end{cases} \quad (6)$$

$$\begin{cases} \delta_{x,L} = [1 \quad \delta_x^2]^T, \delta_{y,L} = [\delta_y \quad \delta_y^2 \quad \delta_y^3]^T, \delta_{z,L} = [\delta_z \quad \delta_z^2]^T \\ \delta_{x,D} = [1 \quad \delta_x^2]^T, \delta_{y,D} = [\beta \delta_y \quad \delta_x^2]^T, \delta_{z,D} = [\delta_z \quad \delta_z^2]^T \\ \delta_{y,N} = \delta_y, \beta_N = \beta \\ \delta_{x,mx} = \delta_x, \beta_{mx} = \beta \\ \delta_{y,my} = \delta_y, \beta_{my} = \beta \\ \delta_{x,mz} = [1 \quad \delta_x^2 \quad \delta_x^4]^T, \delta_{z,mz} = [\delta_z \quad \delta_z^2]^T \\ \xi_L = [1 \quad \xi]^T, \xi_D = [\xi \quad \xi^2]^T, \xi_{mz} = [\xi \quad \xi^2 \quad \xi^3 \quad \xi^4 \quad \xi^5]^T \end{cases} \quad (7)$$

where ξ and Ma denote the span morphing rate and Mach. δ_x, δ_y and δ_z represent the roll elevator deflection, yaw elevator deflection and pitch elevator deflection.

In this paper, the aerodynamic forces and moments are simplified as

$$\begin{cases} L = qS_0 \bar{C}_L^\alpha \alpha + \Delta_L \\ N = qS_0 \bar{C}_N^\beta + \Delta_N \end{cases} \quad (8)$$

$$\begin{cases} M_x = qS_0 L_1 (\bar{m}_x^\beta \beta_{mx} + \bar{m}_x^{\delta_x} \delta_x) + \Delta_{M_x} \\ M_y = qS_0 L_1 (\bar{m}_y^\beta \beta_{my} + c \delta_y) + \Delta_{M_y} \\ M_z = qS_0 L_2 \bar{m}_z (\bar{m}_z^\alpha \alpha + \bar{m}_z^{\delta_z} \delta_z) + \Delta_{M_z} \end{cases} \quad (9)$$

where $\alpha = [1 \quad \alpha \quad \alpha^3]^T$. C_L^α is the partial derivative vector of the lift coefficient for the attack angle. \bar{C}_N^β is the partial derivative of the lateral coefficient for sideslip angle. $\bar{m}_x^\beta, \bar{m}_y^\beta$ and \bar{m}_z^α stand for the partial derivatives of three-axis moment coefficients. $\bar{m}_x^{\delta_x}, \bar{m}_y^{\delta_y}$ and $\bar{m}_z^{\delta_z}$ represent the partial derivatives of the three-axis moment coefficients for the corresponding elevator deflections. $\Delta_L, \Delta_N, \Delta_{M_x}, \Delta_{M_y}$ and Δ_{M_z} represent the inaccuracies in building the model of lift force, drag force, roll moment, yaw moment and pitch moment, respectively.

A scenario has revealed that a complete span morphing leads to a dramatic aerodynamic coefficient change [1]. The results show that the hypersonic morphing vehicle is confident in obtaining much more than 40% moment coefficient increasements in the designed test. The span morphing is a feature of the model. The hypersonic morphing vehicle is able to obtain a great aerodynamic characteristic range, leading to a significantly improved flight envelope. In order to design a robust controller, we should carefully prepare the work.

2.2 Control-oriented model for hypersonic morphing vehicle

The model described by can be divided into two parts. One is the attitude angle subsystem, the other is the angular rate subsystem. The control-oriented model is shown as follows.

$$\begin{cases} \dot{\mathbf{x}}_1 = \mathbf{f}_1 + \mathbf{x}_2 + \mathbf{d}_1 \\ \dot{\mathbf{x}}_2 = \mathbf{f}_2 + \mathbf{g}_2 \mathbf{u} + \mathbf{d}_2 \end{cases} \tag{10}$$

$$\mathbf{g}_1 = \begin{bmatrix} 1 & \sin \alpha \tan \beta & -\cos \alpha \tan \beta \\ 0 & \cos \alpha & \sin \alpha \\ 0 & -\sin \alpha \sec \beta & \cos \alpha \sec \beta \end{bmatrix}$$

$$\mathbf{f}_1(\mathbf{x}_1, \mathbf{x}_2) = \frac{1}{mV} \begin{bmatrix} -L \sec \beta + mg \sec \beta \cos \theta \cos \gamma_V \\ N + mg \cos \theta \sin \gamma_V \\ (\tan \beta + \tan \theta \sin \gamma_V) L + N \tan \theta \cos \gamma_V \end{bmatrix} + \frac{1}{V} \begin{bmatrix} 0 \\ 0 \\ g \cos \theta \tan \beta \sin \gamma_V \end{bmatrix} + (\mathbf{g}_1 - \mathbf{I}) \mathbf{x}_2$$

$$\mathbf{g}_2 = \begin{bmatrix} I_z^{-1} Q S_0 L_2 \bar{m}_z^{\delta_z} \\ I_y^{-1} Q S_0 L_1 \bar{m}_y^{\delta_y} \\ I_x^{-1} Q S_0 L_1 \bar{m}_x^{\delta_x} \end{bmatrix}$$

$$\mathbf{f}_2(\mathbf{x}_1, \mathbf{x}_2) = \begin{bmatrix} I_z^{-1} Q S_0 L_2 \bar{m}_z^\alpha \alpha + I_z^{-1} (I_x - I_y) \omega_x \omega_y \\ I_y^{-1} Q S_0 L_1 \bar{m}_y^\beta \beta_{mx} + I_y^{-1} (I_z - I_x) \omega_x \omega_z \\ I_x^{-1} Q S_0 L_1 \bar{m}_x^\beta \beta_{mx} + I_x^{-1} (I_y - I_z) \omega_y \omega_z \end{bmatrix}$$

where $\mathbf{x}_1 = [\alpha \ \beta \ \gamma_V]^T$, $\mathbf{x}_2 = [\omega_z \ \omega_y \ \omega_x]^T$, $\mathbf{u} = [\delta_z \ \delta_y \ \delta_x]^T$. \mathbf{d}_i , $i = 1, 2$ include the model inaccuracies, external disturbances, the moment of inertia changes and the additional forces and moments.

Further, in order to make tracking error converge within fixed time, the following transformation is introduced.

$$\dot{\mathbf{z}}_1 = \dot{\mathbf{x}}_1 - \dot{\mathbf{x}}_{1c} = \mathbf{f}_1 + \mathbf{x}_2 + \mathbf{d}_1 - \dot{\mathbf{x}}_{1c} \tag{11}$$

Defining $\mathbf{z}_2 = \mathbf{f}_1 + \mathbf{x}_2 - \dot{\mathbf{x}}_{1c}$, and $\mathbf{\Delta}_1 = \mathbf{d}_1$ yields

$$\dot{\mathbf{z}}_1 = \mathbf{z}_2 + \mathbf{\Delta}_1 \tag{12}$$

$$\dot{\mathbf{z}}_2 = \dot{\mathbf{f}}_1 + \mathbf{f}_2 + \mathbf{g}_2 \mathbf{u} + \mathbf{d}_{21} + \mathbf{d}_{22} - \ddot{\mathbf{x}}_{1c} \tag{13}$$

Let $\mathbf{F} = \dot{\mathbf{f}}_1 + \mathbf{f}_2 - \ddot{\mathbf{x}}_{1c}$, $\mathbf{G} = \mathbf{g}_2$, $\mathbf{\Delta}_2 = \mathbf{d}_{21} + \mathbf{d}_{22}$, the model is given as

$$\begin{cases} \dot{\mathbf{z}}_1 = \mathbf{z}_2 + \mathbf{\Delta}_1 \\ \dot{\mathbf{z}}_2 = \mathbf{F} + \mathbf{G} \mathbf{u}(t) + \mathbf{\Delta}_2 \end{cases} \tag{14}$$

3.0 Controller design

Based on the previous discussion, the controller design work for such a nonlinear HMV system with multisource uncertainties is challenging. The hypersonic morphing vehicle can fully utilise the aerodynamic characteristic adjustment caused by wingspan morphing according to the mission and environment. However, the dramatic changes in aerodynamic characteristics demand a controller with outstanding robustness. It is necessary to consider the influence of the multisource uncertainties in the morphing phase because of the flight mission requirement.

The main work in this section is listed as:

- 1) The high-accuracy tracking performance and the closed-loop stability are ensured for the HMV system with the help of the proposed controller method.

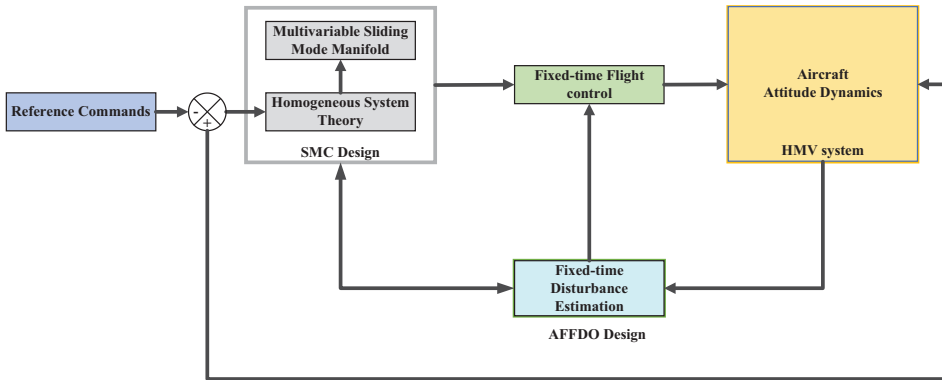


Figure 1. Controller diagram.

- 2) The fuzzy fixed-time disturbance observer ensures the accurate estimation of the multisource uncertainties.

The controller architecture is shown in Fig. 1.

3.1 Preparations for controller design

3.1.1 Assumptions for controller design

The following assumptions are proposed.

Assumption 1 ([31]). *The disturbances are bounded, and the maximum value satisfies*

$$|d_{ij}| \leq D_{ij} \tag{15}$$

Assumption 2 ([32]). *The nonlinear functions f_{ij} , $i = 1, 2, j = 1, 2, 3$ are smooth.*

3.1.2 Definitions

Definition 1. Considering the following nonlinear system

$$\dot{x}(t) = f(x(t)) \tag{16}$$

The system is said to be fixed-time stable, if for any $x(0) \in \Phi$, the solution of the system converges to the origin within a finite time T , and the settling time is bounded $T \leq T_{\max}$ and independent of initial conditions.

Definition 2 ((33)). A function or a vector field is said to be homogenous in the bi-limit if it is homogenous in 0-limit and ∞ – limit simultaneously.

3.1.3 Lemmas

Lemma 1 ([31]). *For the system (16) and a positive function $V(x)$, if there exist some positive parameters $1 < m < 2$, $n = 2 - m$, $l = \frac{\theta}{(m-1)T_c}$, such that*

$$\frac{\dot{V}}{k} \leq -\frac{\theta}{(m-1)T_c} V^{\frac{1+m}{2}} - \frac{1}{(m-1)T_c} V^{\frac{1+n}{2}} \tag{17}$$

then, the trajectory of the system is fixed time stable with a settling time $T \leq 2k^{-1}T_c$.

Proof. The following transformation is employed.

$$\begin{aligned} \frac{\dot{V}}{k} &\leq -\frac{\theta}{(m-1)T_c} V^{\frac{1+m}{2}} - \frac{1}{(m-1)T_c} V^{\frac{1+n}{1}} \\ &= -\frac{1}{(m-1)T_c} \left(\theta V^{\frac{1+m}{2}} + V^{\frac{3-m}{2}} \right) \\ &= -\frac{1}{(m-1)T_c} (\theta V^{m-1} + 1) V^{\frac{3-m}{2}} \end{aligned} \tag{18}$$

Defining $\bar{V} = \theta^{\frac{1}{2}} V^{\frac{m-1}{2}}$ leads to

$$\frac{dV}{dt} \leq -\frac{k}{(m-1)T_c} (\bar{V}^2 + 1) V^{\frac{3-m}{2}} \tag{19}$$

$$\frac{2T_c}{k\theta^{\frac{1}{2}}} \int_{\bar{V}(t_0)}^{\bar{V}(t)} \frac{d\bar{V}}{\bar{V}^2 + 1} \leq t_0 - t \tag{20}$$

By introducing the function $\tan(x)$, one has

$$\arctan[\bar{V}(t)] \leq \arctan[\bar{V}(t_0)] + \frac{k\theta^{\frac{1}{2}}}{2T_c} (t_0 - t) \tag{21}$$

By using $\bar{V}(t) = 0$, the settling time is given by

$$T \leq \frac{2T_c}{k\theta^{\frac{1}{2}}} \arctan[\bar{V}(t_0)] \leq \frac{\pi T_c}{k\theta^{\frac{1}{2}}} = k^{-1}\theta^{-\frac{1}{2}}\pi T_c \tag{22}$$

Choosing parameter $\theta^{\frac{1}{2}} \geq \frac{\pi}{2}$ discloses

$$T \leq 2k^{-1}T_c \tag{23}$$

Therefore, the fixed-time convergence is revealed.

Lemma 2 ([33]). *For system (16), suppose that the vector $f(\mathbf{x})$ is homogeneous in the bi-limit with associate triples (r_p, d_{gp}, f_p) , $p = 0$ or $p = \infty$. If the origins of the system $\dot{\mathbf{x}}(t) = f(\mathbf{x}(t))$, $\dot{\mathbf{x}}_0(t) = f_0(\mathbf{x}(t))$ and $\dot{\mathbf{x}}_\infty(t) = f_\infty(\mathbf{x}(t))$ are global asymptotically stable, then the origin of the system is fixed-time stable in the condition of $d_{g\infty} > 0 > d_{g0}$.*

3.2 AFFDO design

Fuzzy logic system is introduced in the disturbance observer design. The fuzzy rules take the following form [31]:

RULEj: IF x_1 is A_1^j and ... and x_n is A_n^j

THEN y is B^j

where A_1^j, \dots, A_n^j are the fuzzy sets and B^j is the output of the j th fuzzy rules. This research employs the centre-of-gravity defuzzification method to build the output of the fuzzy system.

$$y = \frac{\sum_{j=1}^m E_j \left(\prod_{i=1}^n \Omega_{A_i^j}(x_i) \right)}{\sum_{j=1}^m \left(\prod_{i=1}^n \Omega_{A_i^j}(x_i) \right)} \tag{24}$$

where $\Omega_{A_i^j}(x_i)$ is the fuzzy membership function of variables x_i and κ_j is a singleton fuzzy output value. m is the number of fuzzy rules. Based on the discussion shown above, the output of the fuzzy system is given by

$$y = \kappa^T \psi(x) \tag{25}$$

where $\kappa = [\kappa_1 \cdots \kappa_j \cdots \kappa_m]^T$ is the adjustable parameter vector. $\psi = [\psi_1 \cdots \psi_j \cdots \psi_m]^T$ is the fuzzy basic function vector that is revealed as

$$\psi_j = \frac{\prod_{i=1}^n \Omega_{A_i^j}(x_i)}{\sum_{j=1}^m \left(\prod_{i=1}^n \Omega_{A_i^j}(x_i) \right)} \tag{26}$$

Recalling the results of fuzzy control theory, any real continuous function $f(x)$ defined in a compact set S_c can be approximated by $\sup_{x \in S_c} |\eta^T \psi(x) - f(x)| < \varepsilon$ after applying the fuzzy logic system, where $\varepsilon > 0$ is a small constant.

Based on the above analysis, we employ a fixed-time technique-based adaptive fuzzy fixed-time disturbance observer to estimate the multisource uncertainties and the terms that are difficult to obtain.

The scalar form is adopted to simplify the observer design procedure for $z_1 = [z_{11} \ z_{12} \ z_{13}]^T$. The state and disturbance observers are designed as

$$\dot{\hat{z}}_{1i} = (\tilde{z}_{1i}^2 + 1) \operatorname{sgn}(\tilde{z}_{1i}) \Xi_{1i} + h_{1i} \tag{27}$$

$$\Xi_{1i} = [\lambda_{1,1} |\arctan(\tilde{z}_{1i})|^{p_1} + \lambda_{1,2} |\arctan(\tilde{z}_{1i})|^{q_1} + \lambda_{1,3} |\operatorname{sgn}(\tilde{z}_{1i})|] \tag{28}$$

where $h_{1i} = z_{2i} + \hat{\Delta}_{1i}$ and $\hat{\Delta}_{1i}$ is the i -th element of the disturbance estimation Δ_1 in model (14).

According to the universal approximation feature of the fuzzy logic system, we get

$$\Delta_{1i} = \hat{\Delta}_{1i}(x|\kappa_{1i}^*) + \varepsilon_{1i} \tag{29}$$

where κ_{1i}^* represents the optimal value of κ_{1i} . ε_{1i} is the estimation errors of the fuzzy logic system. By using $\psi_{1i}(x)$ to indicate the fuzzy basic functions, the optimal and nominal estimation of the disturbance can be expressed as

$$\hat{\Delta}_{1i}(x|\kappa_{1i}^*) = \kappa_{1i}^{*T} \psi_{1i}(x) \tag{30}$$

$$\hat{\Delta}_{1i}(x|\hat{\kappa}_{1i}) = \hat{\kappa}_{1i}^T \psi_{1i}(x) \tag{31}$$

where x in the function $\psi_{1i}(x)$ stands for the states in model (10).

Thus, the estimation error is defined as

$$\tilde{z}_{1i} = z_{1i} - \hat{z}_{1i} \tag{32}$$

Thus, the adaptive law is given by

$$\dot{\hat{\kappa}}_{1i} = \lambda_{1,4} \left[\lambda_{1,5} |\arctan(\tilde{z}_{1i})|^{\mu_1} \frac{\operatorname{sgn}(\tilde{z}_{1i})}{1 + \tilde{z}_{1i}^2} \psi_{1i} - \lambda_{1,6} \hat{\kappa}_{1i} \right] \tag{33}$$

where $\mu_1 > 1$.

The state and disturbance observer for $z_2 = [z_{21} \ z_{22} \ z_{23}]^T$ is developed as follows.

$$\dot{\hat{z}}_{2i} = (\tilde{z}_{2i}^2 + 1) \operatorname{sgn}(\tilde{z}_{2i}) \Xi_{2i} + h_{2i} \tag{34}$$

$$\Xi_{2i} = [\lambda_{2,1} |\arctan(\tilde{z}_{2i})|^{p_2} + \lambda_{2,2} |\arctan(\tilde{z}_{2i})|^{q_2} + \lambda_{2,3} |\operatorname{sgn}(\tilde{z}_{2i})|] \tag{35}$$

where $h_{2i} = F_i + (Gu)_i + \hat{\Delta}_{2i}$. $\hat{\Delta}_{2i}$ is the i -th element of the disturbance estimation Δ_2 in model (14).

Employing the fuzzy logic system leads to

$$\Delta_{2i} = \hat{\Delta}_{2i}(x|\kappa_{2i}^*) + \varepsilon_{2i} \tag{36}$$

where κ_{2i}^* is the optimal value of κ_{2i} . ε_{2i} is the estimation error of the fuzzy logic system. The optimal and nominal estimation of the disturbance can be expressed as

$$\hat{\Delta}_{2i}(x|\kappa_{2i}^*) = \kappa_{2i}^{*T} \psi_{2i}(x) \tag{37}$$

$$\hat{\Delta}_{2i}(x|\hat{\kappa}_{2i}) = \hat{\kappa}_{2i}^T \psi_{2i}(x) \tag{38}$$

where $\psi_{2i}(x)$ is the fuzzy basic functions.

Thus, the estimation error is indicated by

$$\tilde{z}_{2i} = z_{2i} - \hat{z}_{2i} \tag{39}$$

One can design the adaptive law as follows.

$$\dot{\hat{\kappa}}_{2i} = \lambda_{2,4} \left[\lambda_{2,5} |\arctan(\tilde{z}_{2i})|^{\mu_2} \frac{\text{sgn}(\tilde{z}_{2i})}{1 + \tilde{z}_{2i}^2} \psi_{2i} - \lambda_{2,6} \hat{\kappa}_{2i} \right] \tag{40}$$

where $\mu_2 > 1$.

Now, the fixed-time observers are successfully developed, where $p_i > 1, 1 > q_i > 0$. $\lambda_{ij}, i = 1, 2, j = 1, 2, 3, 4, 5, 6$ are positive.

3.3 Fuzzy sliding mode controller design

The fixed-time control theory is adopted since the expression of control input can be directly obtained, and the convergence performance can be verified by the Lyapunov theory.

The multivariable fuzzy sliding mode manifold is designed as

$$S(t) = \bar{z}_2 + \int_0^t \sigma_1 d\tau + \int_0^t \sigma_2 d\tau \tag{41}$$

$$\sigma_1 = k_1 [\text{sig}^{p_1}(z_1) + \text{sig}^{q_1}(z_1)] \tag{42}$$

$$\sigma_2 = k_2 [\text{sig}^{p_2}(\bar{z}_2) + \text{sig}^{q_2}(\bar{z}_2)] \tag{43}$$

$$\bar{z}_2 = z_2 + \hat{\Delta}_1 \tag{44}$$

where the parameters are chosen as

$$\begin{cases} p_1 = p \\ p_2 = \rho_0 \end{cases} \tag{45}$$

$$q_1 = q \tag{46}$$

$$q_2 = 2 - \rho_0$$

with the designed coefficients satisfying $\rho_0 \in (0, 1), p \in (0, 1), q > 1$.

Thus, $p_i \in (0, 1)$ and $q_i > 1, i = 1, 2$ is obtained. In this paper, $\text{sig}^p(z_i) = [\text{sig}^p(z_{i1}), \text{sig}^p(z_{i2}), \text{sig}^p(z_{i3})]^T$ and $\text{sig}^r(x) = \text{sign}(x) |x|^r$ are defined.

The derivative of the sliding mode variable S is expressed as

$$\dot{S}(t) = \dot{z}_2 + \dot{\hat{\Delta}}_1 + \sigma_1 + \sigma_2 \tag{47}$$

Substituting the control-oriented model yields

$$\dot{S}(t) = [F + Gu(t) + \Delta_2] + \dot{\hat{\Delta}}_1 + \sigma_1 + \sigma_2 \tag{48}$$

The controller is given as

$$u = G^{-1} [F + \sigma_1 + \sigma_2 + v_{rob}(t) + v_{comp}(t)] \tag{49}$$

$$\mathbf{v}_{rob}(t) = l_1 \mathbf{S} + l_2 \mathbf{sig}^m(\mathbf{S}) + l_3 \mathbf{sig}^n(\mathbf{S}) + l_4 \mathbf{sgn}(\mathbf{S}) \tag{50}$$

$$\mathbf{v}_{comp}(t) = \hat{\mathbf{\Delta}}_2 + \dot{\hat{\mathbf{\Delta}}}_1 \tag{51}$$

where $\hat{\mathbf{\Delta}}_2$ is the output from the observers.

The robust controller is developed in this step.

4.0 Stability analysis

4.1 Convergence of the disturbance estimation

Theorem 1. For the control-oriented model and the designed AFFDO, the estimation error will converge to the origin within fixed-time $T_i \leq 2T_{ic}$, if the key parameters satisfy $\mu_i > 1$, $0 < p_{0,i} < \frac{2}{\mu_i + 1}$, $\lambda_{i,1} = \frac{\theta_i}{(\mu_i + 1)p_{0,i}T_{ic}}$ and $\lambda_{i,2} = \frac{1}{(\mu_i + 1)p_{0,i}T_{ic}}$. The settling time is directly designed in the parameters.

Proof. The Lyapunov function for \tilde{z}_{2i} and $\tilde{\kappa}_{2i}$ is selected as

$$W_2 = \sum_{i=1}^3 \left[|\arctan(\tilde{z}_{2i})|^{\mu_2 + 1} + \frac{1}{2\lambda_{2,4}} \tilde{\kappa}_{2i}^T \tilde{\kappa}_{2i} \right] \tag{52}$$

where $\tilde{\kappa}_{2i} = \kappa_{2i}^* - \hat{\kappa}_{2i}$, $\mu_2 > 1$.

The proof is divided into two stages.

Stage 1. The derivative of the function is represented by

$$\begin{aligned} \dot{W}_2 &= \sum_{i=1}^3 (\mu_2 + 1) |\arctan(\tilde{z}_{2i})|^{\mu_2} \frac{\mathbf{sgn}(\tilde{z}_{2i})}{1 + \tilde{z}_{2i}^2} \left(\dot{\tilde{z}}_{2i} \right) \\ &\quad + \sum_{i=1}^3 \left\{ \tilde{\kappa}_{2i}^T \left[-\lambda_{2,5} |\arctan(\tilde{z}_{2i})|^{\mu_2} \frac{\mathbf{sgn}(\tilde{z}_{2i})}{1 + \tilde{z}_{2i}^2} \boldsymbol{\psi}_{2i} + \lambda_{2,6} \hat{\kappa}_{2i} \right] \right\} \\ &= \sum_{i=1}^3 (\mu_2 + 1) |\arctan(\tilde{z}_{2i})|^{\mu_2} \frac{\mathbf{sgn}(\tilde{z}_{2i})}{1 + \tilde{z}_{2i}^2} \left[\dot{\tilde{z}}_{2i} - (\tilde{z}_{2i}^2 + 1) \mathbf{sgn}(\tilde{z}_{2i}) \boldsymbol{\Xi}_{2i} - h_{2i} \right] \\ &\quad + \sum_{i=1}^3 \left\{ \tilde{\kappa}_{2i}^T \left[-\lambda_{2,5} |\arctan(\tilde{z}_{2i})|^{\mu_2} \frac{\mathbf{sgn}(\tilde{z}_{2i})}{1 + \tilde{z}_{2i}^2} \boldsymbol{\psi}_{2i} + \lambda_{2,6} \hat{\kappa}_{2i} \right] \right\} \end{aligned} \tag{53}$$

With the help of the fuzzy logic system, one gets

$$\begin{aligned} \dot{W}_2 &= \sum_{i=1}^3 (\mu_2 + 1) |\arctan(\tilde{z}_{2i})|^{\mu_2} \frac{\mathbf{sgn}(\tilde{z}_{2i})}{1 + \tilde{z}_{2i}^2} \left[\kappa_{2i}^{*T} \boldsymbol{\psi}_{2i}(x) + \varepsilon_{2i} - (\tilde{z}_{2i}^2 + 1) \mathbf{sgn}(\tilde{z}_{2i}) \boldsymbol{\Xi}_{2i} - \hat{\kappa}_{2i}^T \boldsymbol{\psi}_{2i}(x) \right] \\ &\quad + \sum_{i=1}^3 \left\{ \tilde{\kappa}_{2i}^T \left[-\lambda_{2,5} |\arctan(\tilde{z}_{2i})|^{\mu_2} \frac{\mathbf{sgn}(\tilde{z}_{2i})}{1 + \tilde{z}_{2i}^2} \boldsymbol{\psi}_{2i} + \lambda_{2,6} \hat{\kappa}_{2i} \right] \right\} \end{aligned} \tag{54}$$

$$\begin{aligned} \dot{W}_2 &= \sum_{i=1}^3 (\mu_2 + 1) |\arctan(\tilde{z}_{2i})|^{\mu_2} \frac{\mathbf{sgn}(\tilde{z}_{2i})}{1 + \tilde{z}_{2i}^2} \left[\tilde{\kappa}_{2i}^T \boldsymbol{\psi}_{2i}(x) + \varepsilon_{2i} - (\tilde{z}_{2i}^2 + 1) \mathbf{sgn}(\tilde{z}_{2i}) \boldsymbol{\Xi}_{2i} \right] \\ &\quad + \sum_{i=1}^3 \left\{ \tilde{\kappa}_{2i}^T \left[-\lambda_{2,5} |\arctan(\tilde{z}_{2i})|^{\mu_2} \frac{\mathbf{sgn}(\tilde{z}_{2i})}{1 + \tilde{z}_{2i}^2} \boldsymbol{\psi}_{2i} + \lambda_{2,6} \hat{\kappa}_{2i} \right] \right\} \end{aligned} \tag{55}$$

Choosing parameter $\lambda_{2,5} = \mu_2 + 1$ results in

$$\begin{aligned} \dot{W}_2 &= \sum_{i=1}^3 (\mu_2 + 1) |\arctan(\tilde{z}_{2i})| \frac{\text{sgn}(\tilde{z}_{2i})}{1 + \tilde{z}_{2i}^2} [\varepsilon_{2i} - (\tilde{z}_{2i}^2 + 1) \text{sgn}(\tilde{z}_{2i}) \Xi_{2i}] + \sum_{i=1}^3 [\tilde{\mathbf{k}}_{2i}^T \lambda_{2,6} \hat{\mathbf{k}}_{2i}] \\ &\leq \sum_{i=1}^3 (\mu_2 + 1) |\arctan(\tilde{z}_{2i})| \frac{\text{sgn}(\tilde{z}_{2i})}{1 + \tilde{z}_{2i}^2} \varepsilon_{2i} - \sum_{i=1}^3 (\mu_2 + 1) |\arctan(\tilde{z}_{2i})|^{\mu_2} \Xi_{2i} + \sum_{i=1}^3 [\tilde{\mathbf{k}}_{2i}^T \lambda_{2,6} \hat{\mathbf{k}}_{2i}] \\ &\leq \sum_{i=1}^3 (\mu_2 + 1) |\arctan(\tilde{z}_{2i})|^{\mu_2} \text{sgn}(\tilde{z}_{2i}) \varepsilon_{2i} - \sum_{i=1}^3 (\mu_2 + 1) |\arctan(\tilde{z}_{2i})|^{\mu_2} \Xi_{2i} \\ &\quad + \frac{1}{2} \sum_{i=1}^3 (-\lambda_{2,6} \tilde{\mathbf{k}}_{2i}^T \tilde{\mathbf{k}}_{2i} + \lambda_{2,6} \mathbf{k}_{2i}^* \mathbf{k}_{2i}^*) \end{aligned} \tag{56}$$

Introducing the expression of Ξ_{2i} discloses

$$\begin{aligned} \dot{W}_2 &\leq \sum_{i=1}^3 (\mu_2 + 1) |\arctan(\tilde{z}_{2i})|^{\mu_2} \text{sgn}(\tilde{z}_{2i}) \varepsilon_{2i} - \sum_{i=1}^3 (\mu_2 + 1) \lambda_{2,1} |\arctan(\tilde{z}_{2i})|^{\mu_2 + p_2} \\ &\quad - \sum_{i=1}^3 (\mu_2 + 1) \lambda_{2,2} |\arctan(\tilde{z}_{2i})|^{\mu_2 + q_2} - \sum_{i=1}^3 (\mu_2 + 1) \lambda_{2,3} |\arctan(\tilde{z}_{2i})|^{\mu_2} |\text{sgn}(\tilde{z}_{2i})| \\ &\quad + \frac{1}{2} \sum_{i=1}^3 (-\lambda_{2,6} \tilde{\mathbf{k}}_{2i}^T \tilde{\mathbf{k}}_{2i} + \lambda_{2,6} \mathbf{k}_{2i}^* \mathbf{k}_{2i}^*) \end{aligned} \tag{57}$$

The following parameter is employed

$$\lambda_{2,3} > \max(|\varepsilon_{2i}|) \tag{58}$$

It can be further obtained that

$$\begin{aligned} \dot{W}_2 &\leq - \sum_{i=1}^3 (\mu_2 + 1) \lambda_{2,1} |\arctan(\tilde{z}_{2i})|^{\mu_2 + p_2} - \sum_{i=1}^3 (\mu_2 + 1) \lambda_{2,2} |\arctan(\tilde{z}_{2i})|^{\mu_2 + q_2} \\ &\quad + \frac{1}{2} \sum_{i=1}^3 (-\lambda_{2,6} \tilde{\mathbf{k}}_{2i}^T \tilde{\mathbf{k}}_{2i} + \lambda_{2,6} \mathbf{k}_{2i}^* \mathbf{k}_{2i}^*) \end{aligned} \tag{59}$$

The parameters are transformed to

$$p_2 = 1 + \frac{\mu_2 p_{0,2} + p_{0,2}}{2} \tag{60}$$

$$q_2 = 1 - \frac{\mu_2 p_{0,2} + p_{0,2}}{2} \tag{61}$$

$$1 > \frac{2}{\mu_2 + 1} > p_{0,2} > 0 \tag{62}$$

The derivative of the Lyapunov function is rewritten as

$$\begin{aligned} \dot{W}_2 &\leq - \sum_{i=1}^3 (\mu_2 + 1) \lambda_{2,1} [|\arctan(\tilde{z}_{2i})|^{\mu_2 + 1}]^{1 + \frac{p_{0,2}}{2}} - \sum_{i=1}^3 (\mu_2 + 1) \lambda_{2,2} [|\arctan(\tilde{z}_{2i})|^{\mu_2 + 1}]^{1 - \frac{p_{0,2}}{2}} \\ &\quad + \frac{1}{2} \sum_{i=1}^3 (-\lambda_{2,6} \tilde{\mathbf{k}}_{2i}^T \tilde{\mathbf{k}}_{2i} + \lambda_{2,6} \mathbf{k}_{2i}^* \mathbf{k}_{2i}^*) \end{aligned} \tag{63}$$

Considering the following expression

$$x \leq x^a + x^b \tag{64}$$

where $1 > a > 0, b > 1$.

Therefore

$$\dot{W}_2 \leq - \sum_{i=1}^3 (\mu_2 + 1) \underline{\lambda}_{2,1} |\arctan(\tilde{z}_{2i})|^{\mu_2+1} + \frac{1}{2} \sum_{i=1}^3 (-\lambda_{2,6} \tilde{\mathbf{k}}_{2i}^T \tilde{\mathbf{k}}_{2i} + \lambda_{2,6} \mathbf{k}_{2i}^{*T} \mathbf{k}_{2i}^*) \tag{65}$$

where $\underline{\lambda}_{2,1} = \min\{\lambda_{2,1}, \lambda_{2,2}\}$. Introducing $m_{0,2}$ to indicate $\frac{1}{2} \sum_{i=1}^3 \lambda_{2,6} \mathbf{k}_{2i}^{*T} \mathbf{k}_{2i}^*$ shows

$$\dot{W}_2 \leq - \sum_{i=1}^3 (\mu_2 + 1) \underline{\lambda}_{2,1} |\arctan(\tilde{z}_{2i})|^{\mu_2+1} - \frac{1}{2} \sum_{i=1}^3 (\lambda_{2,6} \tilde{\mathbf{k}}_{2i}^T \tilde{\mathbf{k}}_{2i}) + m_{0,2} \tag{66}$$

Using $\underline{\lambda}_{2,2} = \min\{(\mu_2 + 1) \underline{\lambda}_{2,1}, \lambda_{2,4} \lambda_{2,6}\}$ leads to

$$\dot{W}_2 \leq -\underline{\lambda}_{2,2} W_2 + m_{0,2} \tag{67}$$

Thus, W_2, \tilde{z}_{2i} and $\tilde{\mathbf{k}}_{2i}$ are bounded. The full estimation errors $\bar{\mathbf{e}}_{2i} = \tilde{\mathbf{k}}_{2i}^T \boldsymbol{\psi}_{2i}(x) + \varepsilon_{2i}$ are also bounded.

Stage 2. The Lyapunov function for \tilde{z}_{2i} is designed as follows.

$$V_2 = \sum_{i=1}^3 [|\arctan(\tilde{z}_{2i})|^{\mu_2+1}] \tag{68}$$

The derivative of V_2 is given by

$$\begin{aligned} V_2 &= (\mu_2 + 1) \sum_{i=1}^3 \left[|\arctan(\tilde{z}_{2i})|^{\mu_2} \frac{\text{sgn}(\tilde{z}_{2i}) \dot{\tilde{z}}_{2i}}{1 + \tilde{z}_{2i}^2} \right] \\ &= (\mu_2 + 1) \sum_{i=1}^3 [|\arctan(\tilde{z}_{2i})|^{\mu_2} \Xi_{2i}] + (\mu_2 + 1) \sum_{i=1}^3 |\arctan(\tilde{z}_{2i})|^{\mu_2} \frac{\text{sgn}(\tilde{z}_{2i})}{1 + \tilde{z}_{2i}^2} (\Delta_{2i} - \hat{\Delta}_{2i}) \end{aligned} \tag{69}$$

By introducing the fuzzy logic system, one gets

$$\begin{aligned} \dot{V}_2 &= (\mu_2 + 1) \sum_{i=1}^3 \left[|\arctan(\tilde{z}_{2i})|^{\mu_2} \frac{\text{sgn}(\tilde{z}_{2i}) \dot{\tilde{z}}_{2i}}{1 + \tilde{z}_{2i}^2} \right] \\ &= (\mu_2 + 1) \sum_{i=1}^3 [|\arctan(\tilde{z}_{2i})|^{\mu_2} \Xi_{2i}] + (\mu_2 + 1) \sum_{i=1}^3 |\arctan(\tilde{z}_{2i})|^{\mu_2} \frac{\text{sgn}(\tilde{z}_{2i})}{1 + \tilde{z}_{2i}^2} (\tilde{\mathbf{k}}_{2i}^T \boldsymbol{\psi}_{2i}(x) + \varepsilon_{2i}) \end{aligned} \tag{70}$$

Substituting the expression Ξ_{2i} into \dot{V}_2 reveals

$$\begin{aligned} \dot{V}_2 &= (\mu_2 + 1) \sum_{i=1}^3 \left[|\arctan(\tilde{z}_{2i})|^{\mu_2} \frac{\text{sgn}(\tilde{z}_{2i}) \dot{\tilde{z}}_{2i}}{1 + \tilde{z}_{2i}^2} \right] \\ &\leq - \sum_{i=1}^3 (\mu_2 + 1) \lambda_{2,1} |\arctan(\tilde{z}_{2i})|^{\mu_2+p_2} - \sum_{i=1}^3 (\mu_2 + 1) \lambda_{2,2} |\arctan(\tilde{z}_{2i})|^{\mu_2+q_2} \\ &\quad - \sum_{i=1}^3 (\mu_2 + 1) \lambda_{2,3} |\arctan(\tilde{z}_{2i})|^{\mu_2} |\text{sgn}(\tilde{z}_{2i})| + (\mu_2 + 1) \sum_{i=1}^3 |\arctan(\tilde{z}_{2i})|^{\mu_2} \text{sgn}(\tilde{z}_{2i}) (\tilde{\mathbf{k}}_{2i}^T \boldsymbol{\psi}_{2i}(x) + \varepsilon_{2i}) \end{aligned} \tag{71}$$

Then, the following condition for $\lambda_{2,3}$ is adopted

$$\lambda_{2,3} > \max\{\max(|\varepsilon_{2i}|), \max(|\bar{\mathbf{e}}_{2i}|)\} \tag{72}$$

It leads to

$$\dot{V}_2 \leq - \sum_{i=1}^3 (\mu_2 + 1) \lambda_{2,1} |\arctan(\tilde{z}_{2i})|^{\mu_2+p_2} - \sum_{i=1}^3 (\mu_2 + 1) \lambda_{2,2} |\arctan(\tilde{z}_{2i})|^{\mu_2+q_2} \tag{73}$$

Choosing the following parameters

$$\lambda_{2,1} = \frac{\theta_2}{(\mu_2 + 1) p_{0,2} T_{2c}} \tag{74}$$

$$\lambda_{2,2} = \frac{1}{(\mu_2 + 1) p_{0,2} T_{2c}} \tag{75}$$

The derivative of the Lyapunov function is rewritten

$$\begin{aligned} \dot{V}_2 &\leq - \frac{1}{p_{0,2} T_{2c}} \sum_{i=1}^3 \theta_2 [|\arctan(\tilde{z}_{2i})|^{\mu_2+1}]^{1+\frac{p_{0,2}}{2}} - \frac{1}{p_{0,2} T_{2c}} \sum_{i=1}^3 [|\arctan(\tilde{z}_{2i})|^{\mu_2+1}]^{1-\frac{p_{0,2}}{2}} \\ &\leq - \frac{\theta_2}{p_{0,2} T_{2c}} 3^{-\frac{p_{0,2}}{2}} V_2^{1+\frac{p_{0,2}}{2}} - \frac{1}{p_{0,2} T_{2c}} V_2^{1-\frac{p_{0,2}}{2}} \end{aligned} \tag{76}$$

Introducing $\bar{\theta}_2^2 = \theta_2 3^{-\frac{p_{0,2}}{2}}$, $V_{2,\bar{\theta}_2}^2 = \bar{\theta}_2^2 \left(V_2^{\frac{p_{0,2}}{2}}\right)^2$ and lemma 1, it is obvious that the estimation error will converge to the origin within fixed time. The settling time is estimated by

$$T_2 \leq 2T_{2c} \tag{77}$$

Therefore, \hat{z}_2 tracks z_2 for any time $t \geq T_2$. Note that the disturbance observers have a similar structure. Using the same method, it is easy to demonstrate the fixed time convergence of \tilde{z}_1 . For sake of saving space, the details are omitted.

Since the state estimation error will converge to origin within fixed time T_i for any state z_{ij} , the following expression is established according to the control-oriented model and the disturbance observer.

$$\dot{\tilde{z}}_{ij} = z_{ij} - (\tilde{z}_{ij}^2 + 1) \operatorname{sgn}(\tilde{z}_{ij}) \Xi_{ij} - h_{ij} = \Delta_{ij} - \hat{\Delta}_{ij} = 0 \tag{78}$$

Therefore, we can conclude the disturbance estimation tracks the actual disturbance in the fixed time T_i .

The convergence of the adaptive fuzzy fixed-time disturbance observer is illustrated via Lyapunov theory. It is feasible to achieve disturbance compensation.

Remark 1. In research [34], a fixed time controller is successfully proposed, achieving the significant development. This method has been successfully applied to hypersonic vehicles in [37]. The settling time is estimated by

$$T_f \leq \left(\frac{1}{\lambda_2(p-1) \varepsilon^{p-1}} + \frac{2(\sqrt{n}\varepsilon)^{\frac{1}{2}}}{\lambda_1} \right) \left(1 + \frac{M}{m \left(1 - \frac{\sqrt{2\alpha}}{\lambda_1}\right)} \right) \tag{79}$$

It is clear that the method in this paper leads to a more explicit settling time compared to the result in [34] since the latter is composed of several parameters. These parameters contribute to converge rate. If a specific convergence time is demanded in the design procedure, it is complicated to finish the work. Thus, one can conclude the convergence time of disturbance observer and the sliding mode variable can be directly specified in the design procedure. The stability of the sliding mode variable will be demonstrated later.

4.2 Convergence of the tracking error

Theorem 2. For the control-oriented model, the sliding mode variable will converge to the origin within fixed-time if the parameters satisfy $2 > m > 1$, $n = 2 - m$, $l_2 = \frac{c_1}{(m-1)T_d}$, $l_3 = \frac{1}{(m-1)T_d}$. The settling time satisfies $T \leq T_d$, which is more explicit than the conventional fixed-time control.

Proof. We firstly illustrate the convergence of the sliding mode variable.

$$V_3 = S^T S \tag{80}$$

The derivative is of the designed Lyapunov function is

$$\frac{\dot{V}_3}{2} = S^T \dot{S} \tag{81}$$

Taking the expression of the sliding mode variable results in

$$\begin{aligned} \frac{\dot{V}_3}{2} &= S^T (\dot{z}_2 + \dot{\hat{\Delta}}_1 + \sigma_1 + \sigma_2) \\ &= S^T [F + Gu(t) + \sigma_1 + \sigma_2 + \Delta_2 + \dot{\hat{\Delta}}_1] \end{aligned} \tag{82}$$

Substituting the designed controller shows

$$\begin{aligned} \frac{\dot{V}_3}{2} &= S^T [F + \sigma_1 + \sigma_2 + \Delta_2 + \dot{\hat{\Delta}}_1] - S^T G [G^{-1}(F + \sigma_1 + \sigma_2 + v_{rob} + v_{comp})] \\ &= S^T (\Delta_2 - \hat{\Delta}_2) - S^T v_{rob}(t) \end{aligned} \tag{83}$$

Since the disturbances are eliminated for any time $t > T_1 + T_2$, one gets

$$\frac{\dot{V}_3}{2} = -S^T [l_1 S + l_2 sig^m(S) + l_3 sig^n(S) + l_4 sgn(S) - \tilde{\Delta}_2] \tag{84}$$

The $\tilde{\Delta}_2$ is the full estimation error of the fuzzy logic system. It is obvious that $|\tilde{\Delta}_2|$ is proven to be zero when one illustrates the stability of the adaptive fuzzy fixed-time disturbance observer.

It brings out

$$\begin{aligned} \frac{\dot{V}_3}{2} &\leq -l_1 S^T S - l_2 S^T sig^m(S) - l_3 S^T sig^n(S) \\ &\leq -l_2 S^T sig^m(S) - l_3 S^T sig^n(S) \\ &= -l_2 \sum_{i=1}^3 |s_i| |s_i|^m - l_3 \sum_{i=1}^3 |s_i| |s_i|^n \end{aligned} \tag{85}$$

In order to obtain the fixed-time convergence of the sliding mode variable, the following parameters is introduced.

$$2 > m > 1 \tag{86}$$

$$n = 2 - m \tag{87}$$

$$l_2 = \frac{c_1}{(m-1)T_d} \tag{88}$$

$$l_3 = \frac{1}{(m-1)T_d} \tag{89}$$

Therefore,

$$\begin{aligned} \frac{\dot{V}_3}{2} &\leq -l_2 3^{\frac{1-m}{2}} \left(\sum_{i=1}^3 |s_i|^2 \right)^{\frac{m+1}{2}} - l_3 \left(\sum_{i=1}^3 |s_i|^2 \right)^{\frac{m+1}{2}} \\ &\leq -l_2 3^{\frac{1-m}{2}} V_3^{\frac{m+1}{2}} - l_3 V_3^{\frac{m+1}{2}} \\ &\leq \frac{c_1}{(m-1)T_d} 3^{\frac{1-m}{2}} V_3^{\frac{m+1}{2}} - \frac{1}{(m-1)T_d} V_3^{\frac{3-m}{2}} \end{aligned} \tag{90}$$

with $\bar{c}_1^2 = c_1 3^{\frac{1-m}{2}}$, $V_{3,\bar{c}_1}^2 = \bar{c}_1^2 \left(V_3^{\frac{m-1}{2}} \right)^2$ and lemma 1, the sliding mode will converge to the origin within following settling time.

$$T_3 \leq T_d \tag{91}$$

Theorem 3. *After the convergence of the sliding mode variable and the estimation errors, the tracking error will converge to the origin within fixed-time according to the control-oriented mode of the HMV.*

Proof. Since $S = 0$ is valid, one gets

$$\begin{cases} \dot{z}_1 = z_2 + \Delta_1 = z_2 + \hat{\Delta}_1 + \tilde{\Delta}_1 \\ z_2 + \hat{\Delta}_1 = -\int_0^t \sigma_1 d\tau - \int_0^t \sigma_2 d\tau \end{cases} \tag{92}$$

The fixed-time convergence of the estimation error has been proven, leading to $\tilde{\Delta}_1 = 0$. We obtain the following expression by defining $\bar{z}_1 = z_1$.

$$\begin{cases} \dot{\bar{z}}_1 = \bar{z}_2 \\ \dot{\bar{z}}_2 = -k_1 [\text{sig}^{p_1}(\bar{z}_1) + \text{sig}^{q_1}(\bar{z}_1)] \\ -k_2 [\text{sig}^{p_2}(\bar{z}_2) + \text{sig}^{q_2}(\bar{z}_2)] \end{cases} \tag{93}$$

In this step, the homogeneous system theory is introduced to demonstrate the stability of tracking error.

The system can be rewritten as

$$\dot{\bar{z}} = \begin{bmatrix} \bar{z}_2 \\ -\mathbf{h}_1 & -\mathbf{h}_2 \end{bmatrix} \tag{94}$$

where $\mathbf{h}_1 = [h_{11} \ h_{12} \ h_{13}]^T$, $\mathbf{h}_2 = [h_{21} \ h_{22} \ h_{23}]^T$.

For the case 1: $\bar{z}_{ij} \in \{\bar{z}_{ij} \in R / \{0\} : |\bar{z}_{ij}| \leq 1\}$

$$\begin{aligned} h_{ij} &= k_i \text{sig}^{p_i}(\bar{z}_{ij}) + k_i \text{sig}^{q_i}(\bar{z}_{ij}) \\ &= k_i \left(1 + |\bar{z}_{ij}|^{q_i - p_i} \right) \text{sig}^{p_i}(\bar{z}_{ij}) \end{aligned} \tag{95}$$

For the case 2: $\bar{z}_{ij} \in \{\bar{z}_{ij} \in R / \{0\} : |\bar{z}_{ij}| > 1\}$

$$\begin{aligned} h_{ij} &= k_i \text{sig}^{p_i}(\bar{z}_{ij}) + k_i \text{sig}^{q_i}(\bar{z}_{ij}) \\ &= k_i \left(1 + |\bar{z}_{ij}|^{p_i - q_i} \right) \text{sig}^{q_i}(\bar{z}_{ij}) \end{aligned} \tag{96}$$

Considering the range of $|\bar{z}_{ij}|^{q_i - p_i}$ and $|\bar{z}_{ij}|^{p_i - q_i}$. For the case 1, $2k_i \text{sig}^{p_i}(\bar{z}_{ij}) \geq h_{ij} > k_i \text{sig}^{p_i}(\bar{z}_{ij})$ holds for case 1 and $2k_i \text{sig}^{q_i}(\bar{z}_{ij}) \geq h_{ij} > k_i \text{sig}^{q_i}(\bar{z}_{ij})$ for case 2, respectively.

Then, the homogeneous degree concept is employed to demonstrate the practical fixed-time convergence of the tracking error.

First, the system will be demonstrated to be homogeneous in the 0-limit. The approximation function vector is given by

$$\dot{\bar{z}}_0 = h_0(\bar{z}) = \begin{bmatrix} \bar{z}_2 \\ -k_1 \mathbf{sig}^{p_1}(\bar{z}_1) \quad -k_2 \mathbf{sig}^{p_2}(\bar{z}_2) \end{bmatrix} \tag{97}$$

The associated triple is disclosed by following equations.

$$\begin{cases} r_0^2 = r_0^1 + k_{d0} \\ r_0^2 p_2 = r_0^1 p_1 \\ r_0^2 p_2 = r_0^2 + k_{d0} \end{cases} \tag{98}$$

After fully considering the parameter range, $k_{d0} = -1$ is an acceptable result. Meanwhile, the weight vector is given as $[(2 - p_2)(1 - p_2)^{-1}1 - p_2]^T$. Secondly, the system will be proved to be homogeneous in the ∞ – limit. The following approximation function could be established.

$$\dot{\bar{z}}_\infty = h_\infty(\bar{z}) = \begin{bmatrix} \bar{z}_2 \\ -k_1 \mathbf{sig}^{q_1}(\bar{z}_1) \quad -k_2 \mathbf{sig}^{q_2}(\bar{z}_2) \end{bmatrix} \tag{99}$$

It is obvious to obtain

$$\begin{cases} r_\infty^2 = r_\infty^1 + k_{d\infty} \\ r_\infty^2 p_2 = r_\infty^1 p_1 \\ r_\infty^2 p_2 = r_\infty^2 + k_{d\infty} \end{cases} \tag{100}$$

It is feasible to obtain a set of parameters. $k_{d\infty} = 1$ is an acceptable result. Meanwhile, the weight vector is obtained as $[p_2(1 - p_2)^{-1}(1 - p_2)^{-1}]^T$. Thus, one could conclude that the approximation function vectors are homogeneous in the 0-limit and ∞ – limit, respectively. It is obvious that the system is bi-limit homogeneous. Furthermore, based on the results in [35, 36], it is easy to demonstrate the approximation function vectors are globally asymptotically stable equilibrium. Considering the homogeneous degree satisfies $k_{d0} < 0 < k_{d\infty}$, the fixed-time convergence of the closed-loop system with proper parameters could be verified. The parameters should make the polynomial $N(z) = z^2 - k_2s + k_1$ become a Hurwitz polynomial based on the lemma 2.

The proof is completed.

5.0 Simulation

To verify the effectiveness of the proposed controller, several mathematical simulations are designed. The multisource uncertainties are fully considered, which brings challenges to controller design.

This section presents simulation results by hypersonic flights with continuous morphing. The span variant rate is generated by the step command that passes through a two-order filter.

The following reference commands are employed by applying a second-order filter $\frac{1}{0.07s^2 + 0.5s + 1}$ in case 1.

$$\alpha_c = \begin{cases} 8^\circ, 0 < t < 10 \\ 2^\circ, 10 < t < 20 \\ 8^\circ, 20 < t < 30 \\ 2^\circ, 30 < t < 40 \end{cases} \tag{101}$$

$$\beta_c = 0^\circ, 0 < t < 40 \tag{102}$$

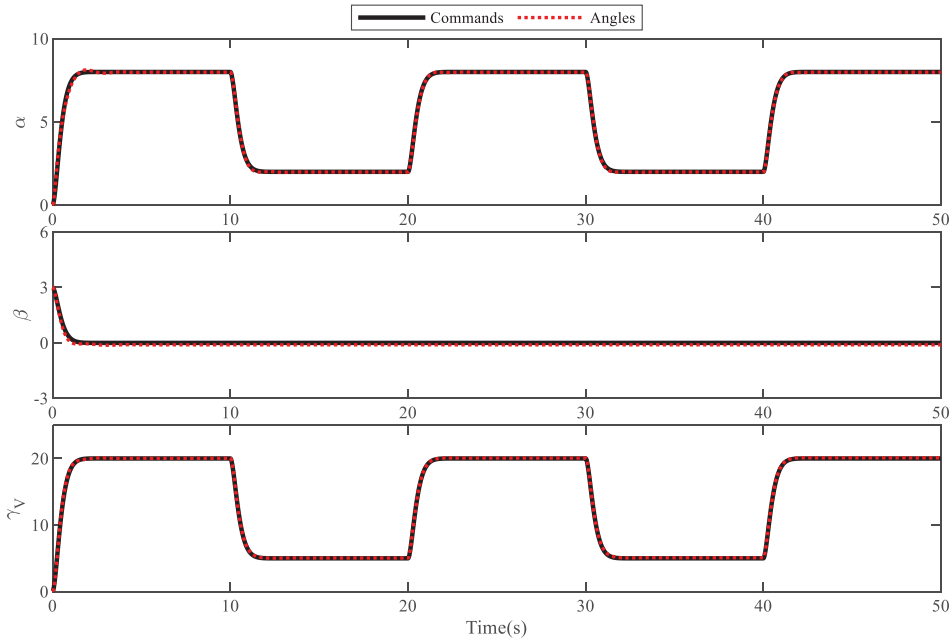


Figure 2. Commands and attitude angles.

$$\gamma_{vc} = \begin{cases} 20^\circ, & 0 < t < 10 \\ 5^\circ, & 10 < t < 20 \\ 20^\circ, & 20 < t < 30 \\ 5^\circ, & 30 < t < 40 \end{cases} \quad (103)$$

The second-order actuator $\frac{1}{0.02s^2 + 0.3s + 1}$ is adopted to generate the span morphing rate $\xi \in [0, 1]$.

The hypersonic morphing vehicle is initialised as $\alpha(t_0) = 0$, $\beta(t_0) = 3$, $\gamma_V(t_0) = 0$, $V = 9Ma$, $H = 30km$ and other states are zero at $t_0 = 0$.

Recalling the principles for the complete control system, which are conditions under (40), guidelines in (45) and (46), and requirements in theorem 1, (60)–(62), (72) and (74)–(75), the designed parameters are given as

$k_1 = 2$, $k_2 = 9.3$, $p_1 = 0.6$, $p_2 = 0.5$, $q_1 = 1.4$ and $q_2 = 1.5$ for the sliding mode manifold.

$c_1 = 1.4$, $T_d = 2.5$, $m = 1.4$, $n = 0.6$ $l_1 = 2$, $l_2 = 1$, $l_3 = 30$, $l_4 = 0.5$ and $l_5 = 10$ for the controller.

$\lambda_{13} = 0.1$, $\lambda_{14} = 1000$, $\lambda_{15} = 12$, $\lambda_{16} = 0.001$, $p_{0,2} = 0.6$, $T_{1c} = 3$, $\theta_1 = 5$, $\mu_1 = 1.1$, $\lambda_{23} = 0.1$, $\lambda_{24} = 4000$, $\lambda_{25} = 3$, $\lambda_{26} = 0.0025$, $p_{0,2} = 0.8$, $T_{2c} = 4$, $\theta_2 = 3.1$ and $\mu_2 = 1.05$ for the fuzzy fixed-time disturbance observer. The fuzzy membership functions are $\Omega_1(x) = (1 + e^{3x+0.5})^{-1}$, $\Omega_2(x) = e^{-(x+0.3)^2}$, $\Omega_3(x) = e^{-(x+0.1)^2}$, $\Omega_4(x) = e^{-x^2}$, $\Omega_5(x) = e^{-(x-0.1)^2}$, $\Omega_6(x) = e^{-(x-0.3)^2}$ and $\Omega_7(x) = (1 + e^{-3x-0.5})^{-1}$. The methods to properly set the FLS is revealed in [31].

5.1 Effectiveness verification

Time-varying commands to reveal the effectiveness of the controller are adopted. The corresponding curves are shown in Figs 2–4. The desired response curves are achieved with the help of the proposed control method under the two consecutive commands and morphing rate changes.

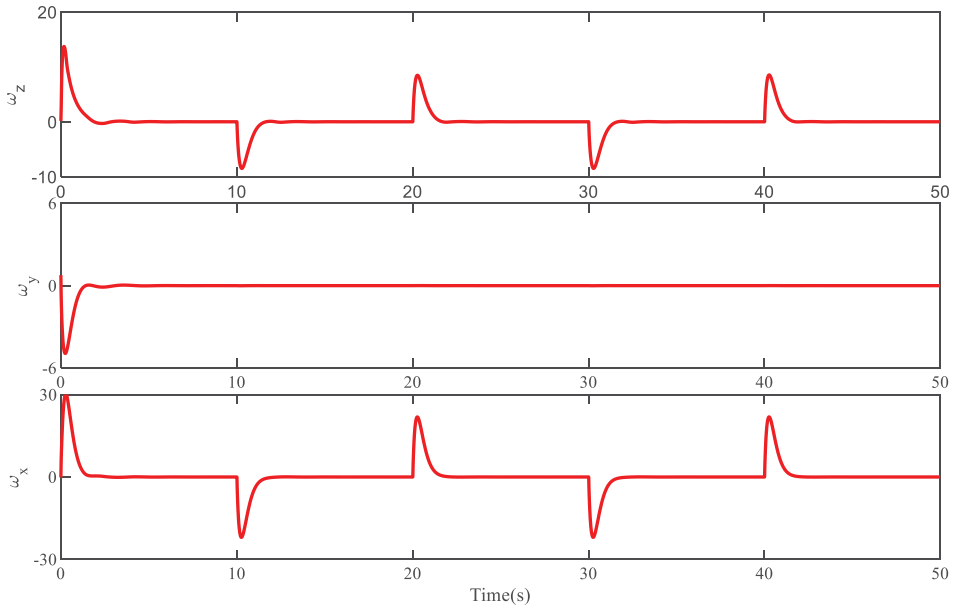


Figure 3. The curves of angular rates.

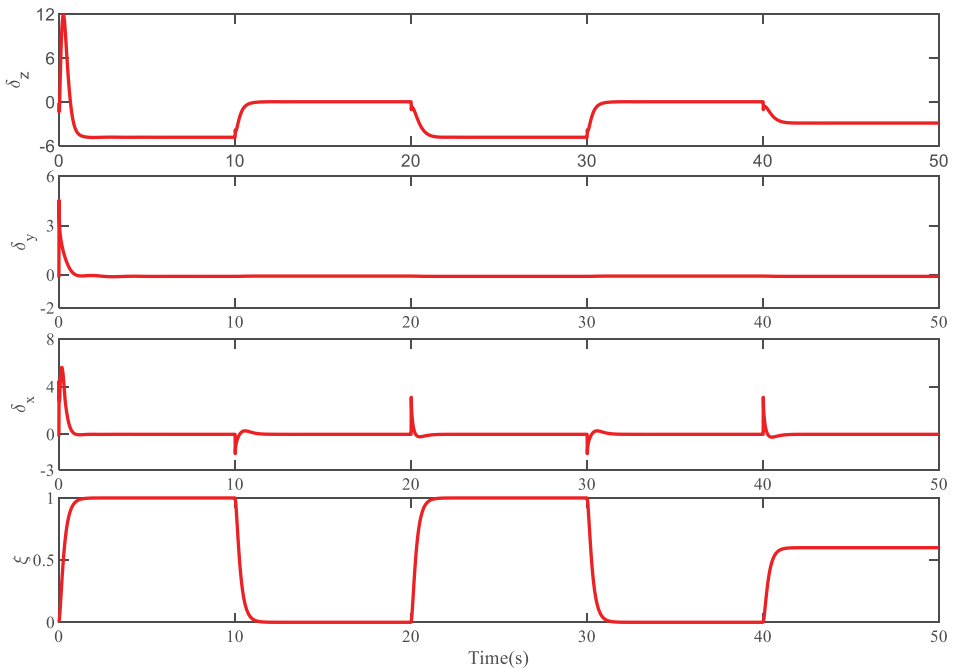


Figure 4. Control inputs and morphing rate.

Figure 1 elaborates on the excellent tracking results of the states. All the attitude angles smoothly track the commands with 2s. Figure 2 reveals the curves of the angular rates. Figure 3 shows the control surfaces and the morphing rate. Since the span morphing influences the aerodynamic characteristic, the steady-state value of the controller changes. The results in this simulation illustrate the effectiveness of the proposed controller. All the angles can accurately track the reference commands within 2.5s

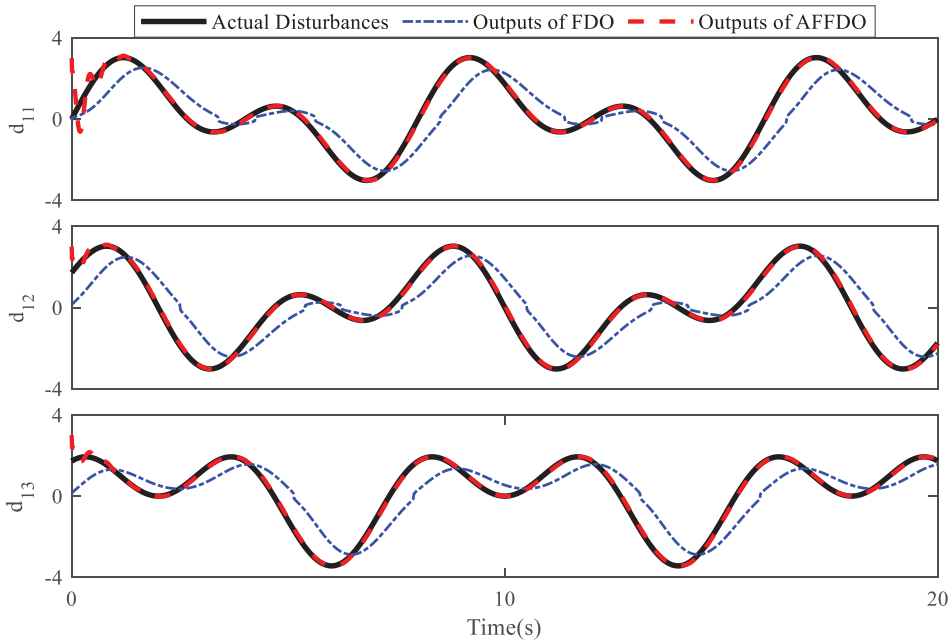


Figure 5. Mismatched disturbance estimations in case 1.

when the HMV is flying in morphing processes. The states are continuous, and the curves of the controllers are acceptable. The varying steady value of δ_z implies the dramatic changes in aerodynamic properties.

5.2 Comparison among different disturbance observers

The disturbance estimations are revealed in this simulation. Therefore, angles and morphing ratio are set to $\alpha = 2^\circ$, $\beta = 0^\circ$, $\gamma_V = 0^\circ$ and $\xi = 0$. The conventional fixed-time disturbance observer and the parameters are obtained from the research [37]. Based on the literature [31], three sets of disturbances are introduced. In case 1, the disturbances are $d_1 = 0.6\Delta_1$ and $d_2 = 0.6\Delta_2$; In case 2, they are $d_1 = 0.8\Delta_1$ and $d_2 = 0.8\Delta_2$; we introduce $d_1 = \Delta_1$ and $d_2 = \Delta_2$ in case 3 with

$$\Delta_1 = \frac{1}{20} \begin{bmatrix} \sin 0.5\pi t \\ \sin 0.5\pi t \\ \cos 0.5\pi t \end{bmatrix} + \frac{1}{20} \begin{bmatrix} \sin 0.25\pi t \\ \cos 0.25\pi t \\ \sin 0.25\pi t \end{bmatrix} \text{ rad/s and } \Delta_2 = 10d_1 \text{ rad/s}^2$$

Figs 5–10 discloses that the estimation of the proposed AFFDO is better than the conventional FDO in the presence of mismatched and matched disturbances. By applying the designed AFFDO, the mismatched disturbances in three cases can be accurately estimated, which is helpful in disturbance compensation. It is announced that the proposed disturbance observer will provide outstanding disturbance estimations without the information on disturbance derivatives, which is necessary for the conventional FDO [37]. Moreover, since the settling time of the proposed methods can be easily pre-specified, the disturbance observer with better convergence performance is available.

5.3 Disturbance compensation demonstration

From the previous simulation, the disturbance estimation performance could be verified. Since matched and mismatched disturbances are inevitable in the flight mission, it is necessary to offer an inspection

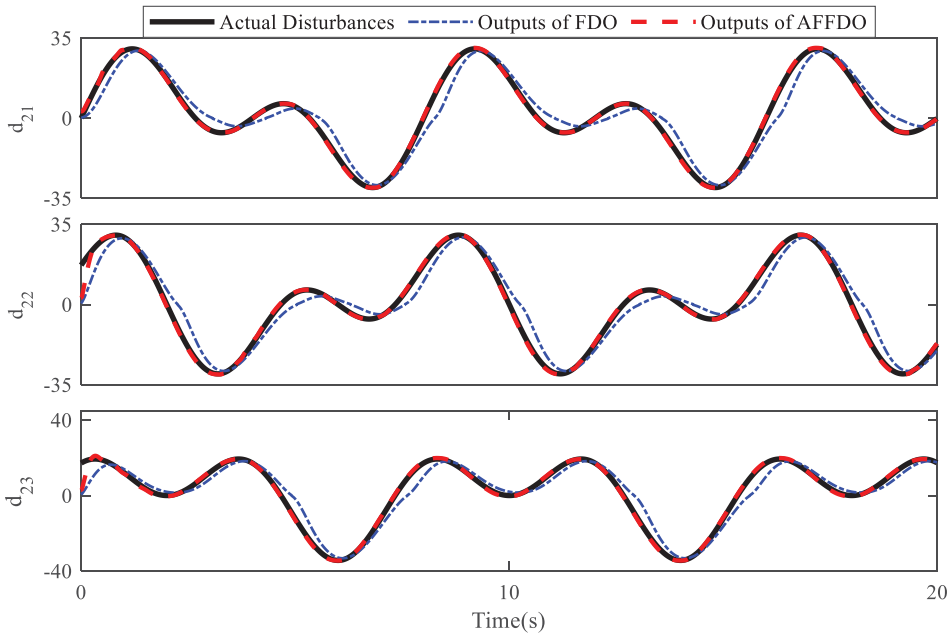


Figure 6. Matched disturbance estimations in case 1.

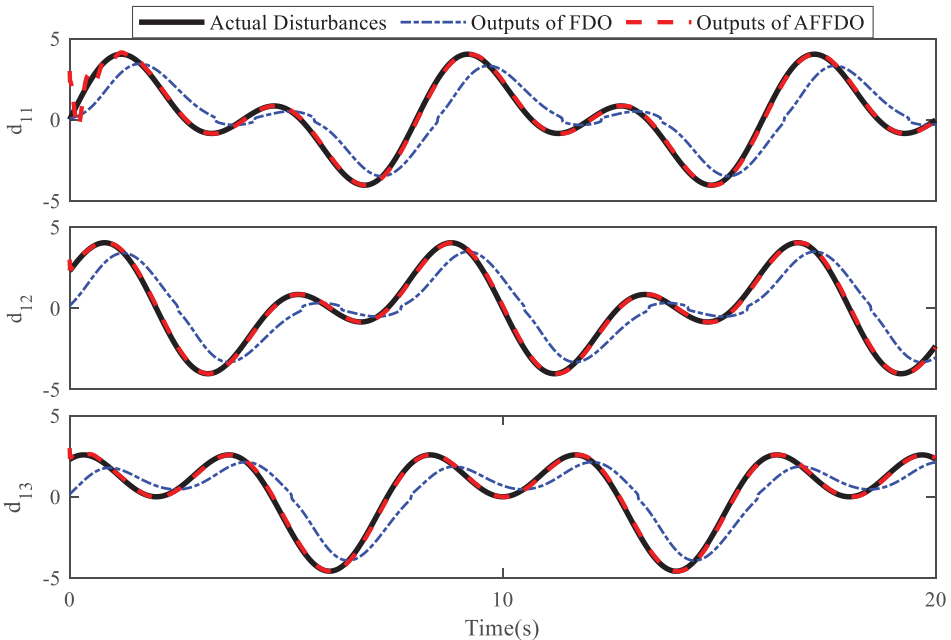


Figure 7. Mismatched disturbance estimations in case 2.

for the controller. Now, we need to demonstrate the disturbance rejection. The proposed fixed-time control without/with the developed AFFDO is designed to test the performance. Figure 11 shows that the anti-disturbance performance is obviously improved by introducing the proposed disturbance observer. Figures 12 and 13 show the angular rates, controller and morphing ratio. According to Figs 14 and 15, we can find that the disturbances are well estimated by the designed disturbance observer. Note that $d_1 = \Delta_1$ and $d_2 = \Delta_2$ are adopted in this simulation.

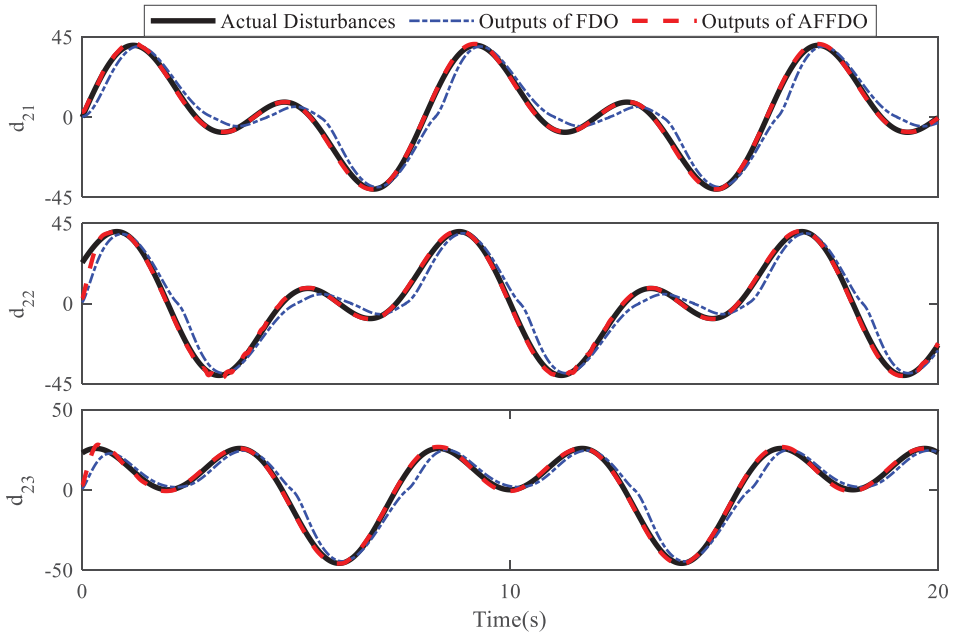


Figure 8. Matched disturbance estimations in case 2.

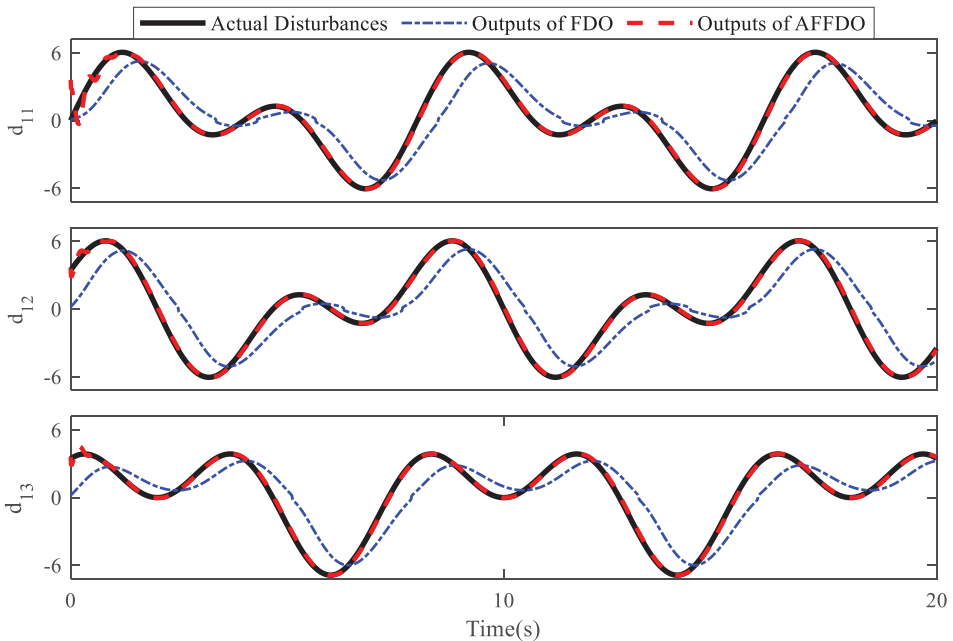


Figure 9. Mismatched disturbance estimations in case 3.

5.4 Comparison among different control methods

Researchers have proposed numerous control methods with different performances. However, for hypersonic morphing vehicles, the controller should have strong robustness and adaptation. The full control method in [37] is chosen to make the comparison, which is indicated by conventional FTC with FDO.

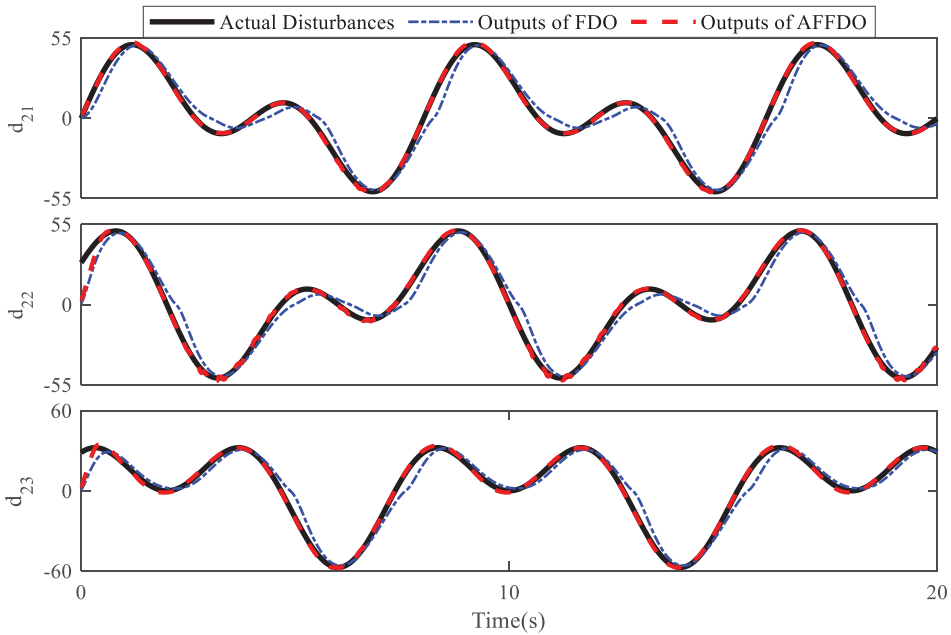


Figure 10. Matched disturbance estimations in case 3.

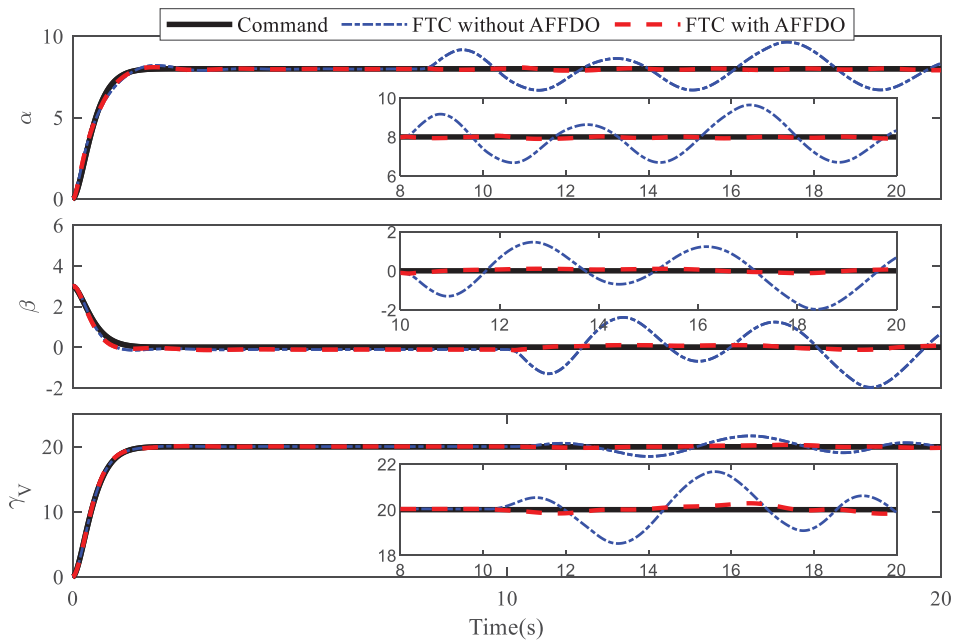


Figure 11. Commands and attitude angles.

d_{11} and d_{21} start to make the impact at $t = 8s$, while the others affect the states from $t = 10s$. The results are shown in Figs 16–20.

Figure 16 shows that the robustness of the proposed control method is better when the proposed strategy is compared with the method in [37]. The different levels of improvement of the tracking

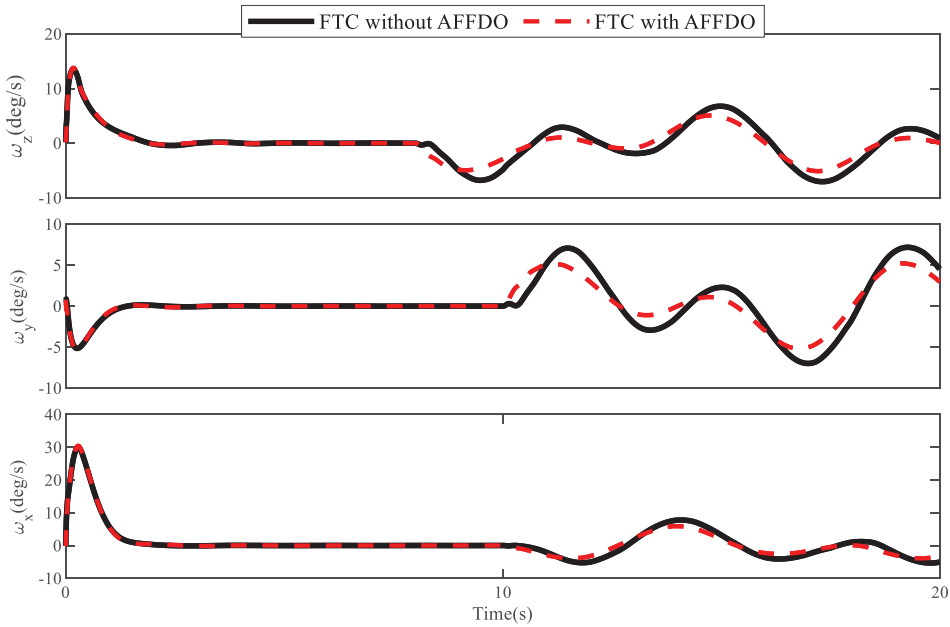


Figure 12. The curves of angular rates.

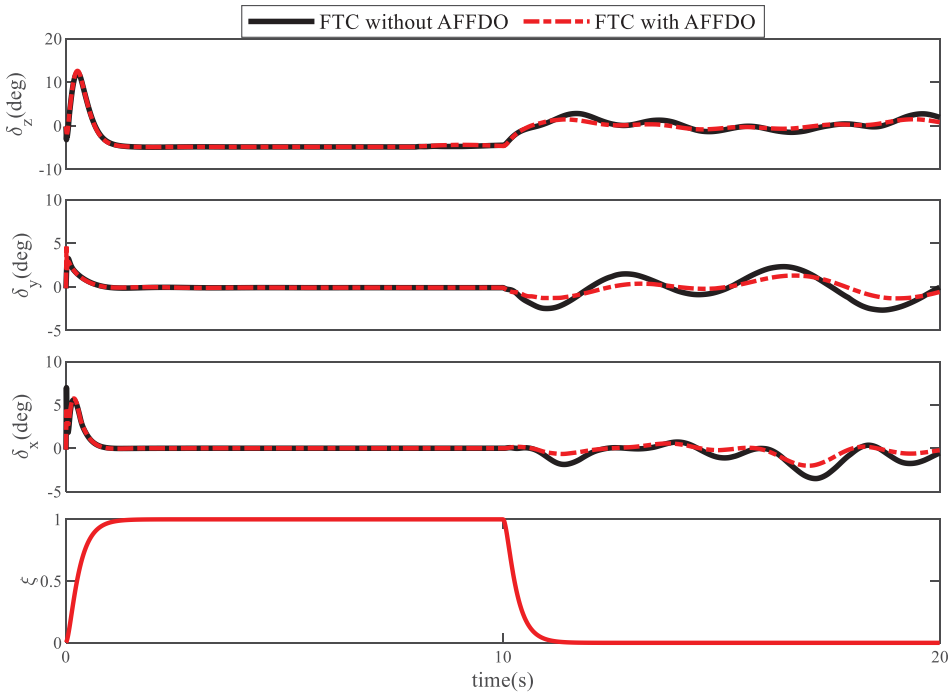


Figure 13. Control inputs and morphing rate.

performance are obtained. Disturbance suppression is ensured by integrating the proposed fuzzy disturbance observer. The proposed control technique has more excellent anti-disturbance performance. Figures 17 and 18 show the corresponding angular rates and the control inputs. Figures 19 and 20 reveal the outputs from the disturbance observers, indicating the different disturbance estimations.

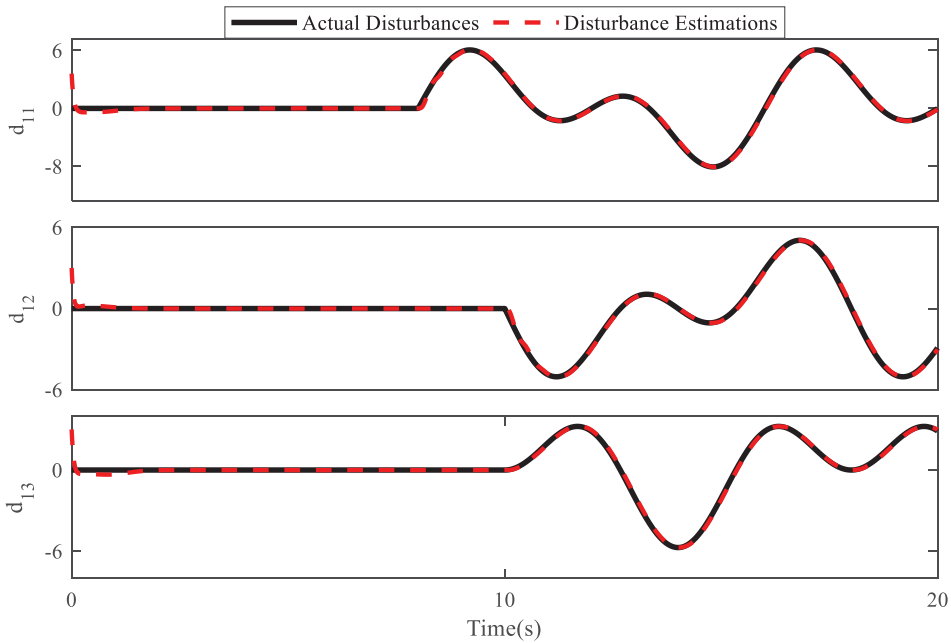


Figure 14. Mismatched disturbance estimations.

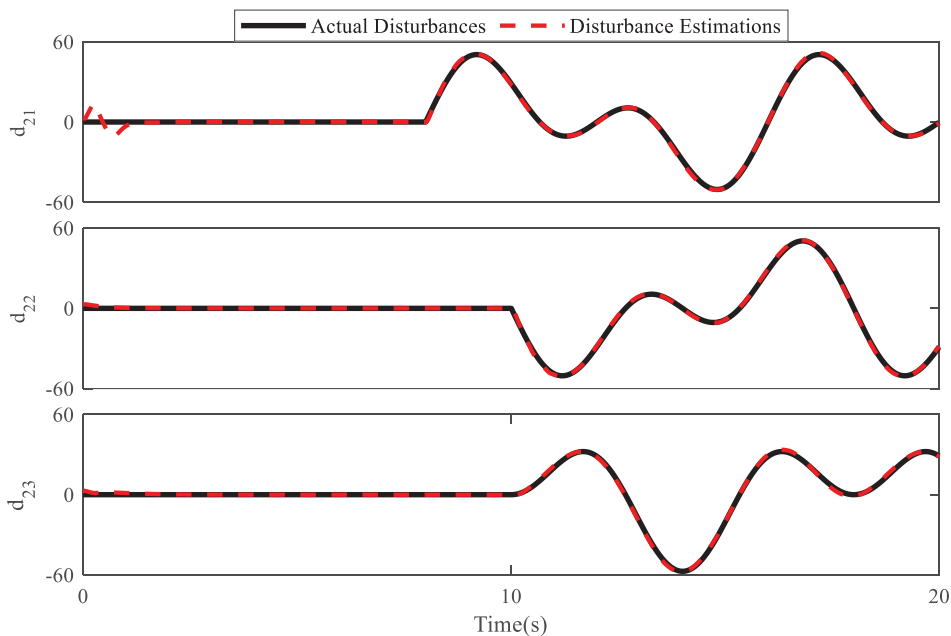


Figure 15. Matched disturbance estimations.

5.5 Control against of aerodynamic parameters perturbations

Since the wingspan morphing technique is introduced, hypersonic morphing vehicles cover a large flight envelop. Therefore, it is important to validate the uncertainties rejection performance. In comparison with the nominal case without any aerodynamic perturbation, the positive perturbation and negative perturbation scenarios are designed to demonstrate the anti-uncertainties performance of the proposed

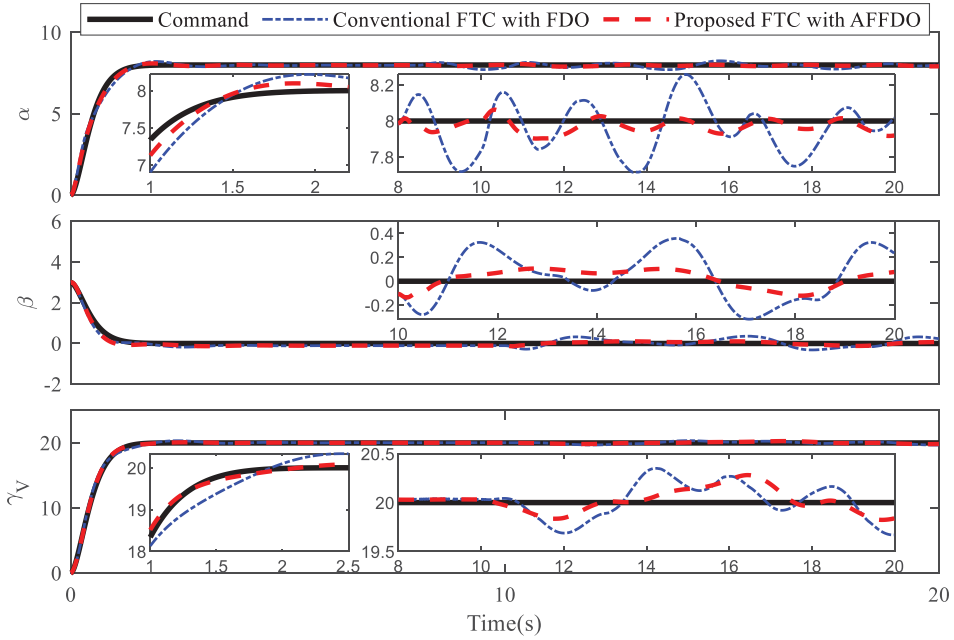


Figure 16. The commands and responses.

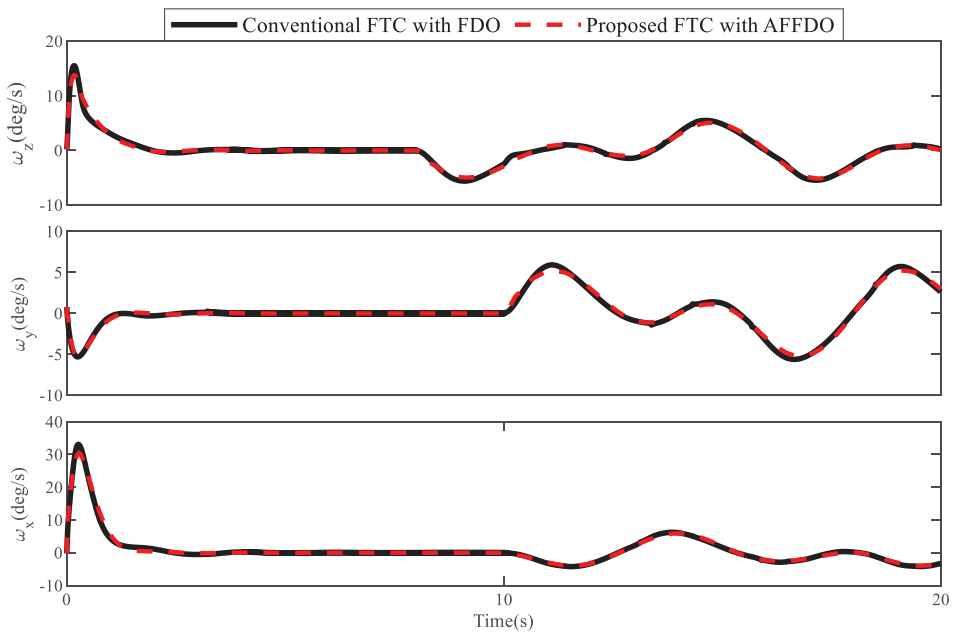


Figure 17. The angular rates.

control method. The atmosphere density perturbation is set to $\pm 20\%$, while the aerodynamic force \bar{C}_L^α , \bar{C}_D^α , \bar{C}_N^β and moment coefficients $\bar{m}_x^{\delta_x}$, $\bar{m}_y^{\delta_y}$, $\bar{m}_z^{\delta_z}$ are perturbed by $\pm 30\%$. The morphing rate is same as the previous simulation.

The results are shown in Figs 21–23. Figure 21 reveals that the positive and negative perturbances impact the convergence procedure of the tracking error. However, all states can get rid of the influence

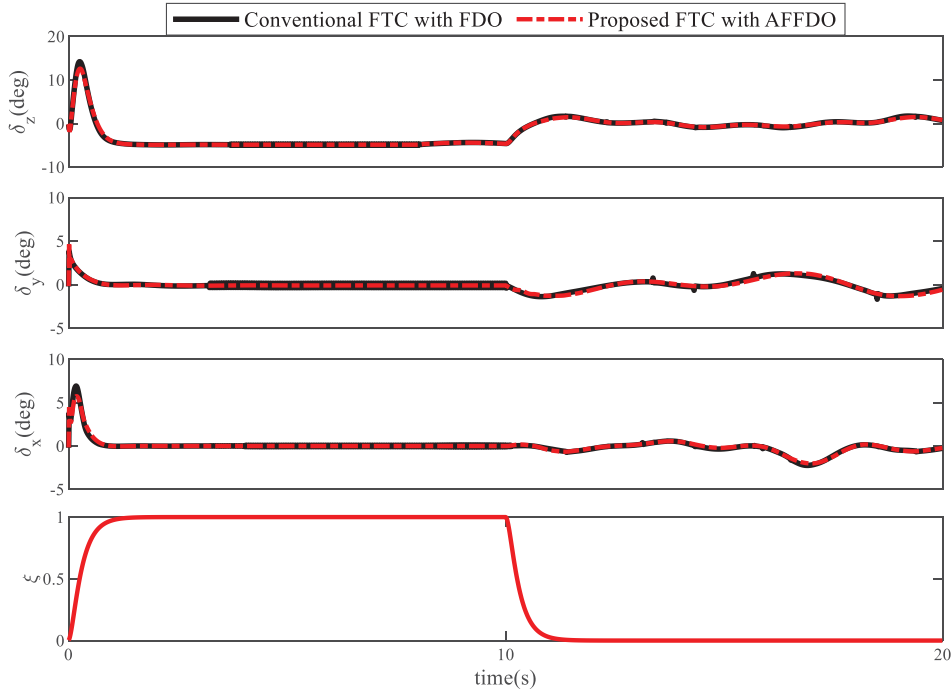


Figure 18. The control inputs and morphing ratio.

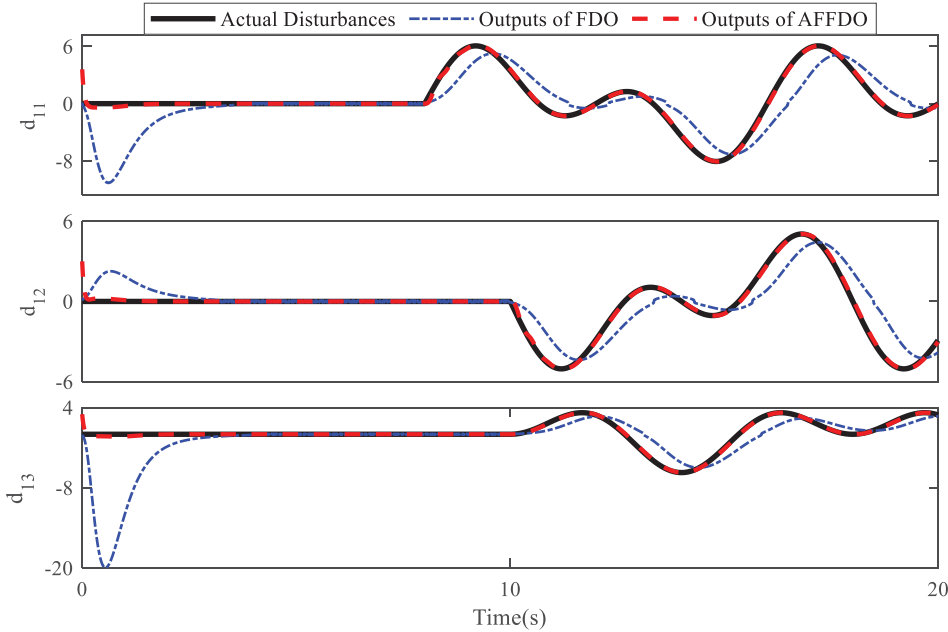


Figure 19. The mismatched disturbance estimations.

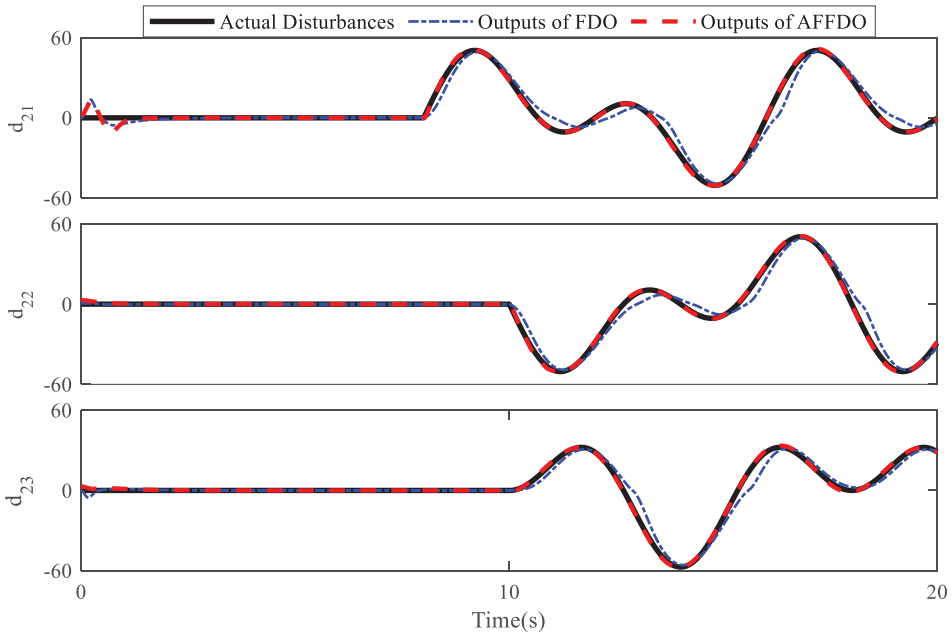


Figure 20. The matched disturbance estimations.

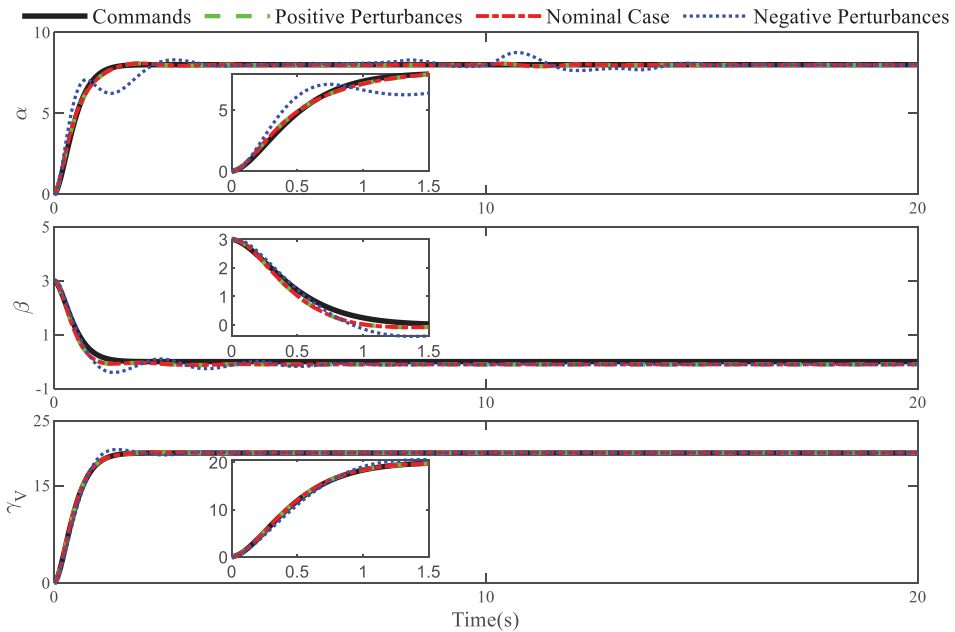


Figure 21. Commands and responses.

of the different perturbances within 2s, which demonstrates the stability of the closed-loop HMV system. Figures 22 and 23 display the corresponding angular rates and the control inputs. In a word, a wide-range flight is achieved for hypersonic morphing vehicles without sacrificing tracking performance in the presence of aerodynamic perturbations.

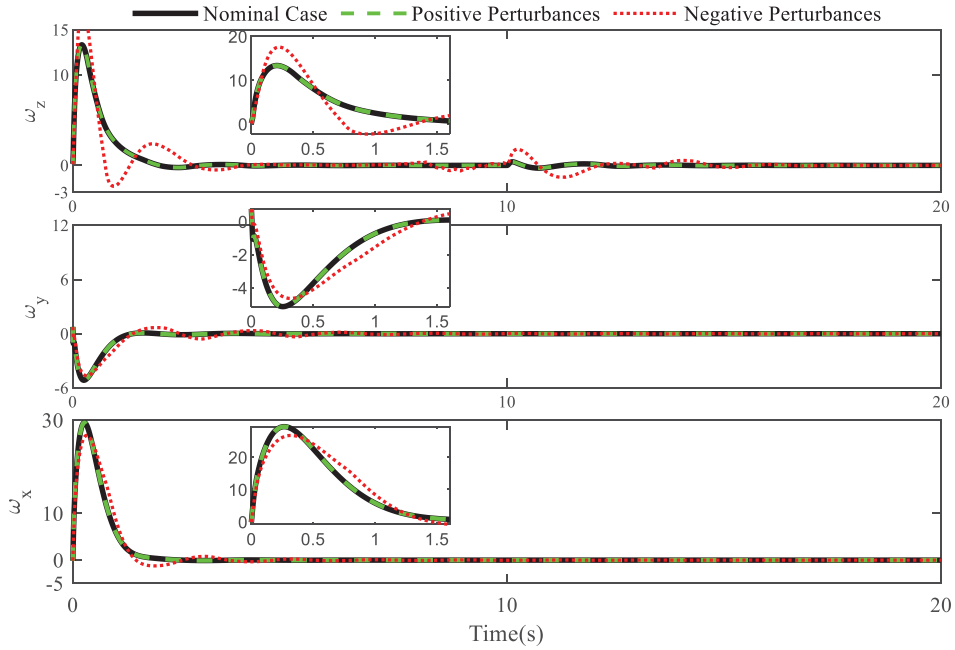


Figure 22. Angular rates.

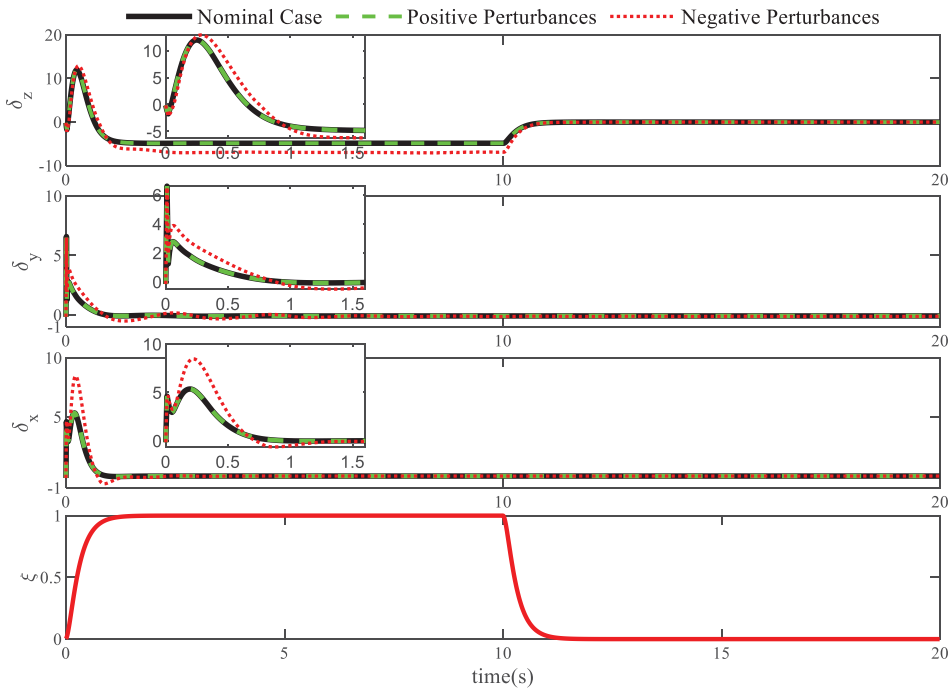


Figure 23. Control inputs and morphing ratio.

6.0 Discussion

A high-accuracy flight control system for HMV has been developed by applying fixed-time control and fuzzy control. The developed fixed-time controller results in an explicit settling time than the traditional fixed-time control method. Moreover, disturbance suppression is achieved without any knowledge of

the disturbance derivatives. Therefore, the anti-disturbance method could be available in engineering applications. The complete flight controller ensures fast and high-accuracy attitude tracking. The results of hypersonic flights in morphing phases match the theoretical findings.

It is necessary to reveal the limitations of the proposed method. The parameters of fuzzy memberships will impact the disturbance estimation. The designed disturbance observer with proper fuzzy memberships will adapt to various disturbances. Inappropriate will deteriorate the disturbance observation. Additionally, the application of the fuzzy logic system will require more computational resources.

Future work will focus on prescribed performance control for HMVs to enhance the flight control performance.

7.0 Conclusions

In this paper, the robust fixed-time controller is constructed to solve the tracking issue for an HMV with multisource uncertainties. The developed control method utilises a fixed-time control technique, homogeneous system theory, and fuzzy logic system to induce the controller. By using the adaptive fuzzy fixed-time disturbance observer, the influence of multisource uncertainties is ideally estimated and compensated. With the help of introducing the homogeneous degree concept, the tracking error converges in a fixed time after the convergence of the multivariable sliding mode variable. The proposed controller has achieved favorable performance in terms of robustness against time multisource uncertainties without the cost of sacrificing the control performance. The Lyapunov theory-based stability analysis is provided to prove the stability of the closed-loop system. The hypersonic morphing vehicle in the morphing phase is studied as the application. Three simulation cases show robustness against disturbance as well as dynamic uncertainties. Future work will consider the development of a prescribed performance controller for hypersonic morphing vehicles.

Funding sources. This work is supported by the National Natural Science Foundation of China Youth Fund (grant number 62003355).

References

- [1] Bao, C., Wang, P. and Tang, G. Integrated method of guidance, control and morphing for hypersonic morphing vehicle in glide phase, *Chin. J. Aeronaut.*, 2021, **34**, (5), pp 535–553. doi: [10.1016/j.cja.2020.11.009](https://doi.org/10.1016/j.cja.2020.11.009)
- [2] Liu, B., Liang, H., Han, Z.-H. and Yang, G. Surrogate-based aerodynamic shape optimization of a morphing wing considering a wide Mach-number range, *Aerosp. Sci. Technol.*, 2022, **124**, p 107557. doi: [10.1016/j.ast.2022.107557](https://doi.org/10.1016/j.ast.2022.107557)
- [3] Liu, Y., Deng, J. and Lu, Y. Preliminary research on optimal design based on control demands for hypersonic morphing vehicle, *IEEE Aerosp. Electr. Syst. Magaz.*, 2013, **28**, (5), pp 23–31. doi: [10.1109/MAES.2013.6516146](https://doi.org/10.1109/MAES.2013.6516146)
- [4] Liu, H., Zhang, Q., Cui, L., Han, X. and Yu, Y. Attitude control of hypersonic morphing aircraft based on incremental backstepping sliding mode, in 2022 7th International Conference on Intelligent Computing and Signal Processing (ICSP), 2022, IEEE, Xi'an, China, pp 1324–1331.
- [5] Liu, H., Zhang, Q., Cui, L., Han, X. and Yu, Y. Attitude control of hypersonic morphing aircraft based on incremental backstepping sliding mode, in 2022 7th International Conference on Intelligent Computing and Signal Processing (ICSP), 2022, IEEE, Xi'an, China, pp 1324–1331. doi: [10.1109/ICSP54964.2022.9778601](https://doi.org/10.1109/ICSP54964.2022.9778601)
- [6] Ding, Y., Yue, X., Chen, G. and Si, J. Review of control and guidance technology on hypersonic vehicle. *Chin. J. Aeronaut.*, 2022, **35**, pp 1–18.
- [7] Ding, Y., Yue, X., Chen, G. and Si, J. Review of control and guidance technology on hypersonic vehicle, *Chin. J. Aeronaut.*, 2022, **35**, (7), pp 1–18. doi: [10.1016/j.cja.2021.10.037](https://doi.org/10.1016/j.cja.2021.10.037)
- [8] Ren, W., Jiang, B. and Yang, H. Singular perturbation-based fault-tolerant control of the air-breathing hypersonic vehicle, *IEEE/ASME Trans. Mechatron.*, 2019, **24**, (6), pp 2562–2571, doi: [10.1109/TMECH.2019.2946645](https://doi.org/10.1109/TMECH.2019.2946645)
- [9] Zhang, X., Hu, W., Wei, C. and Xu, T. Nonlinear disturbance observer based adaptive super-twisting sliding mode control for generic hypersonic vehicles with coupled multisource disturbances, *Eur. J. Contr.*, 2021, **57**, pp 253–262. doi: [10.1016/j.ejcon.2020.06.001](https://doi.org/10.1016/j.ejcon.2020.06.001)
- [10] Lu, Y. Disturbance observer-based backstepping control for hypersonic flight vehicles without use of measured flight path angle, *Chin. J. Aeronaut.*, 2021, **34**, (2), pp 396–406. doi: [10.1016/j.cja.2020.09.053](https://doi.org/10.1016/j.cja.2020.09.053)

- [11] Wang, F., Li, Y., Zhou, C., Zong, Q. and Hua, C. Composite practically fixed time controller design for a hypersonic vehicle with multisource uncertainty and actuator fault, *IEEE Trans. Aerosp. Electron. Syst.*, 2021, **57**, (6), pp 4375–4389. doi: [10.1109/TAES.2021.3103237](https://doi.org/10.1109/TAES.2021.3103237)
- [12] Wang, F., Wen, L., Zhou, C. and Hua, C. Adaptive preassigned-time controller design for a hypersonic vehicle with improved performance and uncertainties, *ISA Trans.*, 2023, **132**, pp 309–328. doi: [10.1016/j.isatra.2022.05.040](https://doi.org/10.1016/j.isatra.2022.05.040)
- [13] Chen, K., Zhu, S., Wei, C., Xu, T. and Zhang, X. Output constrained adaptive neural control for generic hypersonic vehicles suffering from non-affine aerodynamic characteristics and stochastic disturbances, *Aerosp. Sci. Technol.*, 2021, **111**, p 106469. doi: [10.1016/j.ast.2020.106469](https://doi.org/10.1016/j.ast.2020.106469)
- [14] Man, C. and Bai, J. Nonlinear disturbance observer based fuel-consumption optimal control for airbreathing hypersonic vehicles, in 2020 IEEE 16th International Conference on Control & Automation (ICCA), IEEE, Singapore, 2020, pp 1535–1540. doi: [10.1109/ICCA51439.2020.9264493](https://doi.org/10.1109/ICCA51439.2020.9264493)
- [15] Zhao, J., Feng, D., Cui, J. and Wang, X. Finite-time extended state observer-based fixed-time attitude control for hypersonic vehicles, *Mathematics*, 2022, **10**, (17), p 3162. doi: [10.3390/math10173162](https://doi.org/10.3390/math10173162)
- [16] Liu, L., Liu, Y., Zhou, L., Wang, B., Cheng, Z. and Fan, H. Cascade ADRC with neural network-based ESO for hypersonic vehicle, *J. Franklin Inst.*, 2022, p S0016003222006688. doi: [10.1016/j.jfranklin.2022.09.019](https://doi.org/10.1016/j.jfranklin.2022.09.019)
- [17] Wu, T., Wang, H., Yu, Y., Liu, Y. and Wu, J. Quantized fixed-time fault-tolerant attitude control for hypersonic reentry vehicles, *Appl. Math. Modell.*, 2021, **98**, pp 143–160. doi: [10.1016/j.apm.2021.04.033](https://doi.org/10.1016/j.apm.2021.04.033)
- [18] Hu, K.-Y., Wang, X. and Yang, C. Hybrid adaptive dynamic inverse compensation for hypersonic vehicles with inertia uncertainty and disturbance, *Appl. Sci.*, 2022, **12**, (21), p 11032. doi: [10.3390/app122111032](https://doi.org/10.3390/app122111032)
- [19] Yu, C., Jiang, J., Zhen, Z., Bhatia, A.K. and Wang, S. Adaptive backstepping control for air-breathing hypersonic vehicle subject to mismatched uncertainties, *Aerosp. Sci. Technol.*, 2020, **107**, p 106244. doi: [10.1016/j.ast.2020.106244](https://doi.org/10.1016/j.ast.2020.106244)
- [20] Chen, C., Huang, J., Wu, D. and Tu, X. Interval type-2 fuzzy disturbance observer-based T–S fuzzy control for a pneumatic flexible joint, *IEEE Trans. Ind. Electron.*, 2022, **69**, (6), pp 5962–5972. doi: [10.1109/TIE.2021.3090708](https://doi.org/10.1109/TIE.2021.3090708)
- [21] Qiu, J., Wang, T., Sun, K., Rudas, I.J. and Gao, H. Disturbance observer-based adaptive fuzzy control for strict-feedback nonlinear systems with finite-time prescribed performance, *IEEE Trans. Fuzzy Syst.*, 2022, **30**, (4), pp 1175–1184. doi: [10.1109/TFUZZ.2021.3053327](https://doi.org/10.1109/TFUZZ.2021.3053327)
- [22] Zhao, Z., Ren, Y., Mu, C., Zou, T. and Hong, K.-S. Adaptive neural-network-based fault-tolerant control for a flexible string with composite disturbance observer and input constraints, *IEEE Trans. Cyber.*, 2022, **52**, (12), pp 12843–12853. doi: [10.1109/TCYB.2021.3090417](https://doi.org/10.1109/TCYB.2021.3090417)
- [23] Zhao, H.-W. and Yang, L. Global adaptive neural backstepping control of a flexible hypersonic vehicle with disturbance estimation, *AEAT*, 2022, **94**, (4), pp 492–504. doi: [10.1108/AEAT-08-2020-0178](https://doi.org/10.1108/AEAT-08-2020-0178)
- [24] Yu, X., Li, P. and Zhang, Y. Fixed-time actuator fault accommodation applied to hypersonic gliding vehicles, *IEEE Trans. Autom. Sci. Eng.*, 2021, **18**, (3), pp 1429–1440. doi: [10.1109/TASE.2020.3008846](https://doi.org/10.1109/TASE.2020.3008846)
- [25] Ding, Y., Yue, X., Liu, C., Dai, H. and Chen, G. Finite-time controller design with adaptive fixed-time anti-saturation compensator for hypersonic vehicle, *ISA Trans.*, 2022, **122**, pp 96–113. doi: [10.1016/j.isatra.2021.04.038](https://doi.org/10.1016/j.isatra.2021.04.038)
- [26] Guo, J., Yang, S. and Guo, S. Robust tracking for hypersonic vehicles subjected to mismatched uncertainties via fixed-time sliding mode control, *Proc. Inst. Mech. Eng G: J. Aerosp. Eng.*, 2021, **235**, (14), pp 2145–2153. doi: [10.1177/0954410021990239](https://doi.org/10.1177/0954410021990239)
- [27] Tang, X., Zhai, D. and Li, X. Adaptive fault-tolerance control-based finite-time backstepping for hypersonic flight vehicle with full state constraints, *Inf. Sci.*, 2020, **507**, pp 53–66. doi: [10.1016/j.ins.2019.08.012](https://doi.org/10.1016/j.ins.2019.08.012)
- [28] Zhang, X., Zong, Q., Dou, L., Tian, B. and Liu, W. Improved finite-time command filtered backstepping fault-tolerant control for flexible hypersonic vehicle, *J. Franklin Inst.*, 2020, **357**, (13), pp 8543–8565. doi: [10.1016/j.jfranklin.2020.05.017](https://doi.org/10.1016/j.jfranklin.2020.05.017)
- [29] Ding, Y., Yue, X., Chen, G. and Si, J. Review of control and guidance technology on hypersonic vehicle, *Chin. J. Aeronaut.*, 2022, **35**, pp 1–18. doi: [10.1016/j.cja.2021.10.037](https://doi.org/10.1016/j.cja.2021.10.037)
- [30] Dong, Z., Li, Y. and Lv, M. Adaptive nonsingular fixed-time control for hypersonic flight vehicle considering angle of attack constraints, *Int. J. Robust Nonlin Control*, 2023, **33**, pp 6754–6777. <https://doi.org/10.1002/rnc.6722>
- [31] Zhang, H., Wang, P., Tang, G. and Bao, W. Fuzzy disturbance observer-based dynamic sliding mode control for hypersonic morphing vehicles, *Aerosp. Sci. Technol.*, 2023, **142**, pp 108633. <https://doi.org/10.1016/j.ast.2023.108633>
- [32] Zhang, H., Wang, P., Tang, G. and Bao, W. Fixed-time sliding mode control for hypersonic morphing vehicles via event-triggering mechanism, *Aerosp. Sci. Technol.*, 2023, **140**, pp 108458. <https://doi.org/10.1016/j.ast.2023.108458>
- [33] Andrieu, V., Praly, L. and Astolfi, A. Homogeneous approximation, recursive observer design, and output feedback, *SIAM J. Contr. Optimiz.*, 2008, **47**, (4), pp 1814–1850. doi: [10.1137/060675861](https://doi.org/10.1137/060675861)
- [34] Basin, M., Bharath Panathula, C. and Shtessel, Y. Multivariable continuous fixed-time second-order sliding mode control: design and convergence time estimation, *IET Contr. Theory Appl.*, 2017, **11**, (8), pp 1104–1111. doi: [10.1049/iet-cta.2016.0572](https://doi.org/10.1049/iet-cta.2016.0572)
- [35] Perruquetti, W., Floquet, T. and Moulay, E. Finite-time observers: application to secure communication, *IEEE Trans. Automat. Control*, 2008, **53**, (1), pp 356–360. doi: [10.1109/TAC.2007.914264](https://doi.org/10.1109/TAC.2007.914264)
- [36] Yang, F., Wei, C.-Z., Wu, R. and Cui, N.-G. Non-recursive fixed-time convergence observer and extended state observer, *IEEE Access*, 2018, **6**, pp 62339–62351.
- [37] Wang, X., Guo, J., Tang, S. and Qi, S. Fixed-time disturbance observer based fixed-time back-stepping control for an air-breathing hypersonic vehicle, *ISA Trans.*, 2019, **88**, pp 233–245. doi: [10.1016/j.isatra.2018.12.013](https://doi.org/10.1016/j.isatra.2018.12.013)

Appendix A. Variables

Table A1. The indications in the model

Symbols	Description
V	The velocity of the aircraft
g	Gravitational acceleration
$I_k, k = x, y, z$	Pitch, yaw and roll moments of inertia
L, D, N	Lift, drag and lateral forces
$\bar{C}_k, k = L, D, N$	Equivalent aerodynamic coefficients of the forces
$M_k, k = x, y, z$	Pitching, yawing and rolling moments
$\bar{m}_k, k = x, y, z$	Equivalent aerodynamic coefficients of the moments
L_1, L_2	Reference lengths
S, m	The reference area and the mass of the HMV
θ	Flight path angle
ξ	Morphing ratio

Table A2. The symbols in the control-oriented model

Symbols	Description
$\mathbf{x}_1 = [\alpha \quad \beta \quad \gamma_V]^T$	The state consisted of attack angle, sideslip angle and bank angle.
$\mathbf{x}_2 = [\omega_z \quad \omega_y \quad \omega_x]^T$	The state consisted of angular rates of three channels.
$\mathbf{u} = [\delta_z \quad \delta_y \quad \delta_x]^T$	The control input vector consisted of three-channel control fins.
\mathbf{d}_1	The mismatched disturbance consisted of modelling inaccuracies and external disturbances.
\mathbf{d}_2	The matched disturbance, containing model inaccuracies, additional moments and external disturbances.

Table A3. The definitions in the sliding mode controller

Symbols	Description
z	Tracking error.
S	Sliding mode variables.
$\text{sig}(\bullet)$	For $\boldsymbol{\varsigma} = [\varsigma_1 \quad \varsigma_2 \quad \dots \quad \varsigma_n]$, $\text{sig}(\boldsymbol{\varsigma}) = [\text{sig}(\varsigma_1) \quad \text{sig}(\varsigma_2) \quad \dots \quad \text{sig}(\varsigma_n)]$ is defined.

Table A4. The symbols in the disturbance observer

Symbols	Description
$\hat{z}_1, \hat{z}_2, \tilde{z}_1, \tilde{z}_2$	State estimations and the estimation errors
$\hat{\mathbf{d}}_1, \hat{\mathbf{d}}_2, \tilde{\mathbf{d}}_1, \tilde{\mathbf{d}}_2$	Disturbance estimations and the estimation errors
$\psi_{ij}(x), i = 1, 2, j = 1, 2, 3$	Fuzzy basic function
$\mathbf{k}_{ij}, \mathbf{k}_{ij}^*, \hat{\mathbf{k}}_{ij}$	The essential parameters of fuzzy logic system, their desired values and the estimations
$\Omega_{\mathcal{A}_i}$	Fuzzy membership functions

Cite this article: Zhang H., Wang P., Tang G. and Bao W. (2024). Disturbance observer-based fixed-time control for hypersonic morphing vehicles with uncertainties. *The Aeronautical Journal*, **128**, 1844–1874. <https://doi.org/10.1017/aer.2023.116>